IEEE Open Journal of Vehicular Technology

Received 26 March 2024; accepted 18 April 2024. Date of publication 24 April 2024;
date of current version 16 May 2024. The review of this article was coordinated by Editor Shabnam Sodagari.

Digital Object Identifier 10.1109/OJVT.2024.3392951

Relay-Aided Uplink NOMA Under Non-Orthogonal CCI and Imperfect SIC in 6G Networks

VOLKAN ÖZDURAN [1] (Member, IEEE), NIKOLAOS NOMIKOS [2] (Senior Member, IEEE), EHSAN SOLEIMANI-NASAB [3] (Member, IEEE), IMRAN SHAFIQUE ANSARI [4] (Senior Member, IEEE), AND PANAGIOTIS TRAKADAS [2]

[1]İstanbul University-Cerrahpaşa, 34320 Istanbul, Türkiye
[2]Department of Ports Management and Shipping, National and Kapodistrian University of Athens, 34400 Euboea, Greece
[3]Department of Electrical and Computer Engineering, Graduate University of Advanced Technology, Kerman, Iran
[4]James Watt School of Engineering, University of Glasgow, G12 8QQ Glasgow, U.K.

CORRESPONDING AUTHOR: VOLKAN ÖZDURAN (e-mail: volkan@iuc.edu.tr).

This work was supported by HORSE project, funded by the Smart Networks and Services Joint Undertaking (SNS JU) under the European Union's Horizon Europe research and innovation programme under Grant Agreement Number 101096342 (www.horse-6g.eu).

ABSTRACT Sixth generation (6G) networks must guarantee radio-resource availability for coexisting users and machines. Here, non-orthogonal multiple access (NOMA) can address resource limitations by serving multiple devices on the same spectral and temporal resources. Meanwhile, cooperative relays can mitigate the impact with excessive large- and small-scale fading and interference. Still, to unlock the full potential of NOMA in 6G deployments, its performance must be analyzed under interference-limited scenarios with NOMA communications occuring across multiple cells. In this paper, the detrimental effect of co-channel interference (CCI) from nearby NOMA transmissions on a relay-aided NOMA network is examined. More specifically, randomly deployed CCI terminals communicate using NOMA and degrade the uplink communication. Network performance is thoroughly analyzed for various metrics, considering independent and identically distributed non-orthogonal CCI. Furthermore, for improved performance, transmit power, power allocation, and relay location optimization is presented. This scenario can correspond to Industry 4.0 settings, relying on private networks that can adjust the transmit power of interferers within the network. Our analytical findings are verified through Monte-Carlo simulations, revealing that non-orthogonal CCI degrades the system performance, causing system coding gain losses. Nonetheless, the proposed optimization framework can mitigate the impact of non-orthogonal CCI and ensure improved uplink performance.

INDEX TERMS Sixth generation (6G), co-channel interference (CCI), cooperative relaying, non-orthogonal multiple access (NOMA), performance analysis.

I. INTRODUCTION

The tremendous increase of mobile data traffic and the emerging Internet-of-Things (IoT) service accelerate the need for high-capacity and energy-efficient wireless networks [1]. Also, interference-limited scenarios will be dominant in diverse network topologies [2], [3]. In this context, the success of sixth generation (6G) networks will rely on new communication paradigms, departing from current trends. An attractive technique is non-orthogonal multiple access (NOMA) that provides increased resource allocation flexibility, compared to traditional orthogonal multiple access (OMA). NOMA enables resource sharing between users and exploits their channel power level differences [4], [5]. In terms of operation, in NOMA, the transmitter employs superposition coding while the receivers perform successive interference cancellation (SIC) [6]. Meanwhile, various surveys in [7], [8], [9], [10] have identified important NOMA challenges that must be addressed, such as power allocation optimization, increased energy efficiency, and efficient integration with cooperative relaying.

In this work, we focus on a challenging case that is expected to occur in 6G networks, i.e. the investigation of relay-aided and NOMA-based uplink network performance in settings where co-channel interference (CCI) is introduced by other nodes, communicating through NOMA. Such interference scenarios will be increasingly present in topologies with co-existing users and machines, striving for mass connectivity, as it is the case of Industry 4.0 settings [11], [12], [13], [14]. So, for this novel interference scenario, we thoroughly analyze the uplink network performance and formulate optimization problems to optimize the transmit power, power allocation and relay location parameters in a holistic approach where the sources of interference can participate in the optimization process. The proposed framework can be adopted in private networks that support Industry 4.0 application, flexibly optimizing the transmit power of interferers within the network to improve the performance of a desired industrial service [15], [16], [17].

A. BACKGROUND

In networks with challenging wireless conditions, the adoption of cooperative relaying can mitigate the impact of path-loss, shadowing, and multi-path fading by bringing transmitters and receivers closer to each other, and offering increased diversity [18]. Cooperative relaying has been combined with NOMA in various studies that do not consider the impact of CCI, showing its potential to improve the spectral efficiency of the network and pave the way for mass connectivity. A popular area involves device-to-device communication (D2D). In D2D networks, wireless devices can flexibly assume the role of cooperative relays, avoiding the need for infrastructure-based relays, at the cost of reduced hardware capabilities and resource expenditure to support other users. Such settings have been extensively adopted in cooperative NOMA scenarios, starting from earlier studies, such as [19]. In a D2D setting, the authors in [19] enabled users with strong channels to decode the messages of users with worse channel conditions. Next, user pairs were formed and strong users relayed the decoded messages to the weak users. For a similar case, the work in [20] presented low-complexity power control and user pairing algorithms for cooperative NOMA in a D2D network, solving the optimization problems through decomposition to achieve improved rate and energy efficiency. A topology with multi-antenna nodes was investigated in [21], aiming to increase the rate of cell-edge users through beamforming by the source and a strong user. Furthermore, NOMA allowed two sources to share a relay and establish communication with two destinations by transmitting in parallel [22]. This strategy significantly improved the sum ergodic capacity under perfect and imperfect SIC. Other works have employed NOMA in buffer-aided cooperative networks, and proposed highly flexible hybrid OMA/NOMA algorithms that alleviated instances where SIC was not possible [23], [24]. The study in [25] investigates the outage and average sum-rate performance of full-duplex (FD) decode-and-forward relay-aided uplink NOMA, showing performance gains over conventional OMA and half-duplex (HD) relaying. Still, scenarios with multiple user pairs and CCI have not been investigated. Then, the paper in [26] examines various non-orthogonal schemes for multiple access in aerial networks where drones act as relay nodes, optimizing their position and multiple access parameters for improved sum-rate performance. Next, the authors in [27] present optimal power allocation in NOMA-aided relay networks where the source concurrently transmits two information signals towards an amplify-and-forward (AF) relay, thus establishing end-to-end connectivity with a single destination. Finally, the authors in [28] consider Quality-of-Service (QoS) and power usage constraints, and propose HD cooperative asynchronous NOMA with user relaying, inserting a timing mismatch in the broadcast signal to obtain energy efficiency gains over conventional cooperative NOMA.

However, as the adoption rate of NOMA and network density are expected to increase due to coexisting users and IoT devices, the impact of CCI must be carefully analyzed and mitigated. The energy efficiency of uplink and downlink NOMA under Gaussian-mixture aggregate interference, realistically representing the asynchronism in heterogeneous networks is examined in [29]. In a downlink power domain (PD)-NOMA network under CCI, the work in [30] focuses on a single user, performing signal separation through SIC and reveals that coding gain is reduced due to CCI. For networks where underlay D2D cognitive networks introduce CCI to primary uplink NOMA-based networks, the study in [31] conducted a theoretical analysis, in terms of outage probability, effective rate, and ergodic capacity. Performance results highlighted the impact of the decoding order of the users' signals at the base station and the degrading effect of CCI from the underlay D2D network. In a setting with coexisting users and IoT devices, the authors in [32] design a cooperative interference-aware scheduler to mitigate CCI. Both OMA and NOMA cases are examined and data rate, energy consumption, and capacity gains are obtained over conventional scheduling. Additionally, to enhance the spectrum utilization and system performance, the authors in [33] propose and analyze the performance of short packet NOMA communication for coordinated and direct relay transmission in IoT networks. The CCI and imperfect SIC effects are also considered in the system performance analysis. Next, the paper in [34] investigates the performance of a network, in which two NOMA users communicate through an IoT access point, acting as a relay. For this case, closed-form expressions for the exact and asymptotic outage probability and ergodic data of the NOMA users are derived, considering the impact of CCI and efficient machine learning-aided power allocation strategies are given. Another work studying a NOMA-based network under CCI is presented in [35]. By assuming that the desired signal experiences Rician fading while CCI signals follow Rayleigh fading, the outage performance is analyzed for varying numbers of interferers and traffic loads. Finally, various solutions have been proposed towards pairing together

users, in order to improve the performance of NOMA under CCI. Indicatively, the authors in [36] propose sum-rate-based user-pair scheduling for multi-user information exchange by means of non-orthogonal channels to avoid the inter-cell interference that is caused by other users, in dense wireless networks.

Focusing on relay-aided NOMA networks, various studies analyze the impact of CCI and present relevant mitigation techniques. The authors in [37] investigate HD/FD bi-directional relay-aided uplink/downlink NOMA under independent and identically distributed (i.i.d.) and independent but not identically distributed (i.n.i.d.) CCI. Both perfect/imperfect SIC cases were evaluated, in terms of system outage probability and throughput, showing improved FD relay-aided NOMA performance for perfect SIC. Another interesting CCI case, in a relay-aided NOMA IoT topology was examined in [38]. Here, energy harvesting is adopted to increase the network's lifetime while a source and an IoT relay, concurrently transmit their data to their destinations using NOMA. In this setting, an external entity introduces CCI to the network and the optimal combination of time-switching and power splitting EH is studied to improve the outage and throughput performance. The case of underlay spectrum sharing is the focus of [39], where interference arising from the secondary relay-aided network to the primary-user must be below a pre-defined threshold. The analysis showed that the impact of CCI from the secondary-user transmitter to the primary-user's reception was more severe than that of the relay. Moreover, the use of NOMA in the secondary network was revealed to increase the throughput, compared to OMA. Also, a spectrum sharing scenario with a NOMA-based secondary network is examined in [40]. As multiple relays are available, the far user performance is improved through appropriate duplexing mode selection, exploiting both HD and FD relaying. A similar underlay relay-aided NOMA network is studied in [41]. Here, the CCI from the primary to the secondary network is analyzed under imperfect SIC and imperfect channel state information (CSI). As multiple relays are available in the secondary network, various selection algorithms are presented, as well as a deep learning framework for outage probability and throughput prediction whose output matches the analytical and simulation results. However, these studies, either do not focus on CCI stemming from nearby NOMA transmissions [37], [38] or consider the impact of CCI from NOMA transmissions on the reception of users communicating with OMA [39], [40], [41].

B. CONTRIBUTIONS

As it is evident, relay-aided NOMA networks facilitate the access of edge users and IoT devices in the forthcoming 6G era by leveraging their channel asymmetries and heterogeneous rate requirements. Thus, instances of CCI from NOMA transmissions will become more frequent, threatening network performance. In this paper, contrary to the current state-of-the-art, we present a relay-aided NOMA network that is affected by CCI, arising from nearby NOMA transmissions. To the best of our knowledge, it is the first time that such a setup is investigated, as an analysis on the impact of non-orthogonal CCI on relay-aided NOMA has not yet been presented.

In greater detail, our contributions are as follows:

- The impact of non-orthogonal CCI from randomly deployed terminals on a relay-aided NOMA network with heterogeneous QoS requirements is examined. i.i.d. CCI cases, subject to Rayleigh are studied.
- A thorough theoretical analysis, in terms of outage probability, error probability, throughput, energy efficiency, and diversity order is provided.
- The procedure for optimizing the transmit power, power allocation coefficient for NOMA, and relay location is presented, aiming to minimizing the impact of non-orthogonal CCI on the relay network.
- Performance evaluation through Monte-Carlo simulations is provided, verifying our analytical findings. Moreover, the proposed network optimization procedure demonstrates significant performance improvement for the relay-aided uplink NOMA network.

The derived expressions for the considered performance metrics can facilitate the efficient deployment and evaluation of NOMA-based solutions in the context of 6G networks. It is expected that the dramatic rise in the number of coexisting users, IoT devices and unmanned vehicles, among others, in 6G networks will necessitate the use of non-orthogonal scheme to meet mass connectivity demands above 5G's requirements [42]. As a result, instances of non-orthogonal CCI will be increasingly common in 6G deployments. Moreover, the proposed optimization demonstrated high potential in relay-aided NOMA networks under non-orthogonal CCI cases that will increasingly arise in future communication networks with massive numbers of coexisting users and IoT devices. We expect that such holistic optimization process, involving the sources of interference will be adopted especially in cases where centralized network monitoring and coordination can be applied, as it is the case of private networks, supporting Industry 4.0 environments.

C. STRUCTURE

The remainder of this paper is organized as follows. In Section II, we introduce the system model and the main assumptions. In Section III, we present the theoretical analysis of the relay-aided NOMA network, in terms of outage probability, error probability, throughput, and energy efficiency. Then, Section IV provides the asymptotic expressions for the outage and error probabilities while Section V includes the diversity order analysis for the considered relay network. The optimization steps for the relay location and power allocation are given in Section VI and performance evaluation results are provided in Section VII. Finally, conclusions and future directions are discussed in Section VIII. List of acronyms that are used in the paper are presented in Table 1. List of notations that are used in the paper are presented in the Table 2. The Superscript "up" represents the upper-bound throughout the paper.

TABLE 1. List of Acronyms

AWGN	Additive white Gaussian noise
AF	Amplify-and-Forward
BPSK	Binary phase-shift keying
BS	Base-station
CCI	Co-channel interference
CDF	Cumulative density function
CSI	Channel state information
D2D	Device-to-device
EE	Energy efficiency
EH	Energy harvesting
EP	Error probability
FD	Full-duplex
HD	Half-duplex
i.i.d.	independent and identically distributed
i.n.i.d.	independent but not identically distributed
IoT	Internet-of-Things
NOMA	Non-orthogonal multiple access
OMA	Orthogonal multiple access
PDF	Probability density function
PD-NOMA	Power-domain NOMA
RV	Random variable
QPSK	Quadrature phase-shift-keying
QoS	Quality of service
SE	Spectral efficiency
SIC	Successive interference cancellation
SINR	Signal-to-interference-plus-noise ratio
SNR	Signal-to-noise ratio
OP	Outage probability
6G	Sixth generation

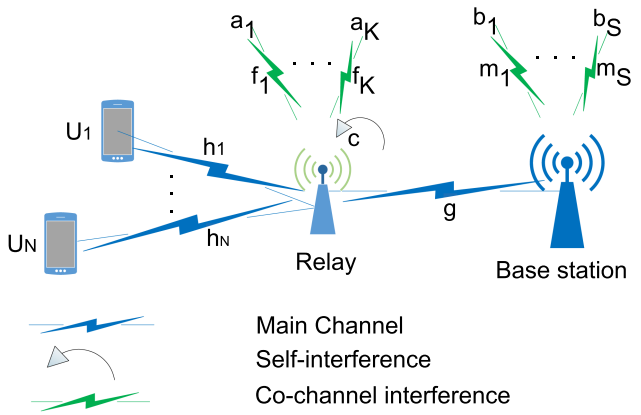

FIGURE 1. Two-hop relay-aided uplink NOMA network affected by non-orthogonal CCI.

II. SYSTEM MODEL & CHANNEL STATISTICS

A two-hop uplink NOMA network, comprising a base station (BS), N users U_i, $\forall_i = 1, \ldots, N$, and HD/FD AF relay R is considered, as depicted in Fig. 1. U_i and BS do not have a direct link due to severe fading and communication is established via the AF-based relay. The adoption of an AF-based

TABLE 2. List of Notation

α_k	Power allocation coefficient for CCI_k
θ_s	Power allocation coefficient for CCI_s
β_i	Power allocation coefficient for U_i
β_N	Power allocation coefficient for U_N
h_i	$\mathrm{U}_i \rightarrow$ Relay channel
h_N	$\mathrm{U}_N \rightarrow$ Relay channel
g	Relay $\rightarrow$ BS channel
c	Loop-interference channel
f_k	$\mathrm{CCI}_k \rightarrow$ Relay channel
m_s	$\mathrm{CCI}_s \rightarrow$ BS channel
Ω_{h_i}	Mean of $\lvert h_i \rvert^2$
Ω_{h_N}	Mean of $\lvert h_N \rvert^2$
Ω_g	Mean of $\lvert g \rvert^2$
Ω_c	Mean of $\lvert c \rvert^2$
Ω_{f_k}	Mean of $\lvert f_k \rvert^2$
Ω_{m_s}	Mean of $\lvert m_s \rvert^2$
$\sigma^2_{h_i}$	Variance of $\lvert h_i \rvert^2$
σ^2_g	Variance of $\lvert g \rvert^2$
σ^2_c	Variance of $\lvert c \rvert^2$
$\sigma^2_{f_k}$	Variance of $\lvert f_k \rvert^2$
$\sigma^2_{m_s}$	Variance of $\lvert m_s \rvert^2$
σ^2	Variance of AWGN
x_i	Information signal of the U_i
x_N	Information signal of the U_N
a_k	Information signal of the CCI_k
b_s	Information signal of the CCI_s
P_S	User's transmit power
P_R	Relay's transmit power
P_F	CCI_k's transmit power
P_M	CCI_s's transmit power
w_R	AWGN noise at Relay
w_{BS}	AWGN noise at BS
λ	Level of residual self-interference
λ_ℓ	Level of residual interference
d_i	$\mathrm{U}_i \rightarrow$ Relay Euclidean distance
d_N	$\mathrm{U}_N \rightarrow$ Relay Euclidean distance
d_k	$\mathrm{CCI}_k \rightarrow$ Relay Euclidean distance
d_s	$\mathrm{CCI}_s \rightarrow$ BS Euclidean distance
ν	Path-loss exponent
B	Bandwidth
τ	Throughput
K	Number of CCIs at Relay
S	Number of CCIs at BS
N	Number of Users
R	Target rate
$\gamma^{HD}_{th,i}$	U_i's target threshold rate in HD mode
$\gamma^{HD}_{th,N}$	U_N's target threshold rate in HD mode
$\gamma^{FD}_{th,i}$	U_i's target threshold rate in FD mode
$\gamma^{FD}_{th,N}$	U_N's target threshold rate in FD mode
$\mathbb{E}[.]$	Expectation operator
$\mathcal{CN}(.,.)$	Complex Gaussian
$R_{th,i}$	Target rate for i-th user

relay stems from its ability to handle the incoming signal without necessitating additional signal decoding and encoding processes that might introduced delays in the relaying process. This characteristic holds significance in the context of ultra-low latency services. It is assumed that each network node is equipped with a single omni-directional antenna while the relay and the BS are affected by a limited number of CCI terminals communicating under the NOMA paradigm.

In this study, h_i and g represent the $U_i \rightarrow R$ and $R \rightarrow BS$ channel coefficients, being complex Gaussian RVs with zero mean and variances $\sigma^2_{h_i}$ and σ^2_g, respectively, i.e. $h_i \sim \mathcal{CN}(0, \Omega_{h_i})$ and $g \sim \mathcal{CN}(0, \Omega_g)$. $c \sim \mathcal{CN}(0, \Omega_c)$ represents the loop-interference that is caused by the simultaneous transmit and receive process in FD mode. In addition, $f_k \sim \mathcal{CN}(0, \Omega_{f_k})$ and $m_s \sim \mathcal{CN}(0, \Omega_{m_s})$ represent the k-th, $\forall_k = 1, \ldots, K$, and s-th, $\forall_s = 1, \ldots, S$, CCI, affecting the relay and the BS, respectively. Each user U_i, $\forall_i = 1, \ldots, N$, transmits the respective signal x_i with $\mathbb{E}\left[|x_i|^2\right] = 1$ and a power allocation coefficient β_i, where $\sum_{i=1}^{N} \beta_i = 1$, to the BS via the HD/FD AF relay.

In this uplink NOMA network, it is considered that the user with the best channel gain is located closer to the relay and the N users are ordered based on $|h_1|^2 \geq, \ldots, \geq |h_N|^2$ while the order of the power allocation coefficients are $1 > \beta_i \geq, \ldots, \geq \beta_N > 0$ [43], [44]. Moreover, considering the effect of path-loss, the U_i's channel variance is redefined as $\Omega_{h_i} = \sigma^2_{h_i} d_i^{-v}$ where d_i represents the $U_i \rightarrow R$ distance and v denotes the path-loss exponent, taking values between $2-6$ [45]. The distance between the k-th CCI terminal and the relay is represented as d_k, while the distances of the set of K CCI terminals towards the relay are ordered as $d_1 \leq d_2 \leq, \ldots, \leq d_K$. Therefore, the k-th CCI terminal $\rightarrow R$ channel variance can be redefined as $\Omega_{f_k} = \sigma^2_{f_k} d_k^{-v}$. Likewise, the distance between the s-th CCI terminal and the BS is represented as d_s while the distances of the set of S CCI terminals towards the BS are ordered as $d_1 \leq d_2 \leq, \ldots, \leq d_S$. As a result, the s-th CCI terminal $\rightarrow BS$ channel variance can be redefined as $\Omega_{m_s} = \sigma^2_{m_s} d_s^{-v}$.

A. SIGNALING

The received signals at the HD/FD relay comprising the NOMA-based signals of the N users and the CCI from K CCI terminals can be written as

$$y_R^{\text{HD}} = \sum_{i=1}^{N} \sqrt{\beta_i P_S} h_i x_i + \sum_{k=1}^{K} \sqrt{\alpha_k P_F} f_k a_k + w_R, \tag{1}$$

$$y_R^{\text{FD}} = \sum_{i=1}^{N} \sqrt{\beta_i P_S} h_i x_i + \sum_{k=1}^{K} \sqrt{\alpha_k P_F} f_k a_k + \sqrt{P_R} c + w_R, \tag{2}$$

where P_S and P_F represent the transmit power of each user terminal and each CCI terminal affecting the relay's reception, respectively. Also, w_R is the additive white Gaussian noise (AWGN) at the relay with variance equal to σ^2. The set of K CCI terminals transmits a superimposed signal introducing the CCI towards the relay with power allocation coefficients $\sum_{k=1}^{K} \alpha_k = 1$, based on $1 > \alpha_1 >, \ldots, > \alpha_K > 0$ and $\mathbb{E}\left[|a_k|^2\right] = 1$.

The amplification factor employed by the AF HD/FD relay denoted by G_{AF} can be calculated as

$$G_{\text{AF}}^{\text{HD}} = \sqrt{\frac{P_R}{\sum_{i=1}^{N} \beta_i P_S |h_i|^2 + \sum_{k=1}^{K} \alpha_k P_F |f_k|^2 + \sigma^2}}, \tag{3}$$

$$G_{\text{AF}}^{\text{FD}} = \sqrt{\frac{P_R}{\psi}}, \tag{4}$$

where $\psi = \sum_{i=1}^{N} \beta_i P_S |h_i|^2 + \sum_{k=1}^{K} \alpha_k P_F |f_k|^2 + P_R |c|^2 + \sigma^2$ and P_R is the relay's transmit power. The set of S CCI terminals transmits a superimposed signal, acting as CCI towards the BS characterized by power allocation coefficients $\sum_{s=1}^{S} \theta_s = 1$, according to $1 > \theta_2 >, \ldots, > \theta_S > 0$ and $\mathbb{E}[|b_s|^2] = 1$. After the amplification process, the received signal at the BS can be written as

$$y_{BS}^{\text{HD}} = G_{\text{AF}} g y_R^{\text{HD}} + \sum_{s=1}^{S} \sqrt{\theta_s P_M} m_s b_s + w_{BS}, \tag{5}$$

$$y_{BS}^{\text{FD}} = G_{\text{AF}} g y_R^{\text{FD}} + \sum_{s=1}^{S} \sqrt{\theta_s P_M} m_s b_s + w_{BS}, \tag{6}$$

where w_{BS} is the AWGN at the BS with variance equal to σ^2 and P_M is the transmit power used by each CCI terminal affecting the BS's reception. Substituting (1) into (5) and (2) into (6), the following expressions can be obtained as

$$\begin{aligned} y_{BS}^{\text{HD}} = {} & G_{\text{AF}}^{\text{HD}} g \sum_{i=1}^{N} \sqrt{\beta_i P_S} x_i h_i + G_{\text{AF}}^{\text{HD}} g \sum_{k=1}^{K} \sqrt{\alpha_k P_F} f_k a_k \\ & + G_{\text{AF}}^{\text{HD}} g w_R + \sum_{s=1}^{S} \sqrt{\theta_s P_M} m_s b_s + w_{BS}. \end{aligned} \tag{7}$$

$$\begin{aligned} y_{BS}^{\text{FD}} = {} & G_{\text{AF}}^{\text{FD}} g \sum_{i=1}^{N} \sqrt{\beta_i P_S} x_i h_i + G_{\text{AF}}^{\text{FD}} g \sum_{k=1}^{K} \sqrt{\alpha_k P_F} f_k a_k \\ & + G_{\text{AF}}^{\text{FD}} g \sqrt{P_R} c + G_{\text{AF}}^{\text{FD}} g w_R + \sum_{s=1}^{S} \sqrt{\theta_s P_M} m_s b_s + w_{BS}. \end{aligned} \tag{8}$$

B. UPLINK RATES AT THE BASE STATION

The signal decoding process is performed by adopting the SIC strategy, according to the order of the power allocation coefficients, which is $1 > \beta_i > \beta_N > 0$, as

$$R_{x_i}^{\text{HD}} = \frac{1}{2} \log \left(1 + \frac{G_{\text{AF}}^{\text{HD},2} |h_i|^2 |g|^2 \beta_i P_S}{A} \right), \tag{9}$$

$$R_{x_N}^{\mathrm{HD}} = \frac{1}{2}\log\left(1+\frac{G_{\mathrm{AF}}^{\mathrm{HD},2}|h_N|^2|g|^2\beta_N P_S}{B}\right), \quad (10)$$

$$R_{x_i}^{\mathrm{FD}} = \log\left(1+\frac{G_{\mathrm{AF}}^{\mathrm{FD},2}|h_i|^2|g|^2\beta_i P_S}{C}\right), \quad (11)$$

$$R_{x_N}^{\mathrm{FD}} = \log\left(1+\frac{G_{\mathrm{AF}}^{\mathrm{FD},2}|h_N|^2|g|^2\beta_N P_S}{D}\right), \quad (12)$$

where $G_{\mathrm{AF}}^{\mathrm{HD},2} = G_{\mathrm{AF,HD}}^2$, $G_{\mathrm{AF}}^{\mathrm{FD},2} = G_{\mathrm{AF,FD}}^2$, and exponent 2 represents an exponentiation process. $A = G_{\mathrm{AF}}^{\mathrm{HD},2}|g|^2 P_S \sum_{j=i+1}^{N-1}\beta_j|h_j|^2 + G_{\mathrm{AF}}^{\mathrm{HD},2}|g|^2\sum_{k=1}^{K}\alpha_k P_F|f_k|^2 + G_{\mathrm{AF}}^{\mathrm{HD},2}|g|^2\sigma^2 + \sum_{s=1}^{S}\theta_s P_M|m_s|^2 + G_{\mathrm{AF}}^{\mathrm{HD},2}\sum_{\ell=1}^{i-1}P_S\beta_\ell|\widehat{h}_\ell|^2|g|^2+\sigma^2$, $B = G_{\mathrm{AF}}^{\mathrm{HD},2}|g|^2\sum_{k=1}^{K}\alpha_k P_F|f_k|^2 + G_{\mathrm{AF}}^{\mathrm{HD},2}\sigma^2|g|^2 + \sum_{s=1}^{S}\theta_s P_M|m_s|^2 + G_{\mathrm{AF}}^{\mathrm{HD},2}\sum_{\ell=1}^{N-1}P_S\beta_\ell|\widehat{h}_\ell|^2|g|^2+\sigma^2$, $C = G_{\mathrm{AF}}^{\mathrm{FD},2}|h_j|^2|g|^2\sum_{j=i+1}^{N-1}\beta_j P_S + G_{\mathrm{AF}}^{FD,2}|g|^2\sum_{k=1}^{K}\alpha_k P_F|f_k|^2 + G_{\mathrm{AF}}^{FD,2}|g|^2 P_R|c|^2 + G_{\mathrm{AF}}^{FD,2}\sigma^2|g|^2 + \sum_{s=1}^{S}\theta_s P_M|m_s|^2 + G_{\mathrm{AF}}^{\mathrm{FD},2}\sum_{\ell=1}^{i-1}P_S\beta_\ell|\widehat{h}_\ell|^2|g|^2+\sigma^2$, and $D = G_{\mathrm{AF}}^{\mathrm{FD},2}|g|^2\sum_{k=1}^{K}\alpha_k P_F|f_k|^2 + G_{\mathrm{AF}}^{FD,2}|g|^2 P_R|c|^2 + G_{\mathrm{AF}}^{FD,2}\sigma^2|g|^2 + \sum_{s=1}^{S}\theta_s P_M|m_s|^2 + G_{\mathrm{AF}}^{\mathrm{FD},2}\sum_{\ell=1}^{N-1}P_S\beta_\ell|\widehat{h}_\ell|^2|g|^2+\sigma^2$. Note that there will be some level of residual interference because of imperfect SIC that is caused by the SIC process of each user. In this regard, $\sum_{\ell=1}^{q-1}\sqrt{P_S\beta_\ell}\widehat{h}_\ell$. $q \in \{j, N\}$, $\widehat{h}_\ell \sim \mathcal{CN}(0, \lambda_\ell\Omega_{\widehat{h}_\ell})$ represents the imperfect SIC terms. The λ_ℓ represents the level of residual interference and takes values between $0 \le \lambda_\ell \le 1$ [46], [47]. Substituting $G_{\mathrm{AF}}^{\mathrm{HD/FD}}$ from (3) and (4), into (9), (10), (11), and (12), and after some mathematical manipulations, the following expressions can be obtained

$$R_{x_i}^{\mathrm{HD}} = \frac{1}{2}\log\left(1+\frac{\beta_i\gamma_{x_i}\gamma_y}{\Psi_1+\Psi_2}\right), \quad (13)$$

$$R_{x_N}^{\mathrm{HD}} = \frac{1}{2}\log\left(1+\frac{\beta_N\gamma_{x_N}\gamma_y}{\Delta_1+\Delta_2}\right), \quad (14)$$

$$R_{x_i}^{\mathrm{FD}} = \log\left(1+\frac{\beta_i\gamma_{x_i}\gamma_y}{\Lambda_1+\Lambda_2}\right), \quad (15)$$

$$R_{x_N}^{\mathrm{FD}} = \log\left(1+\frac{\beta_N\gamma_x\gamma_y}{\Upsilon_1+\Upsilon_2}\right), \quad (16)$$

where $\gamma_{x_i} = \frac{P_S|h_i|^2}{\sigma^2}$, $\gamma_{x_N} = \frac{P_S|h_N|^2}{\sigma^2}$, $\gamma_y = \frac{P_R|g|^2}{\sigma^2}$, $\gamma_{x_j} = \frac{P_S|h_j|^2}{\sigma^2}$, $\gamma_J = \sum_{j=i+1}^{N-1}\gamma_{x_j}$, $\gamma_F = \frac{\sum_{k=1}^{K}P_F|f_k|^2}{\sigma^2}$, $\gamma_M = \frac{\sum_{s=1}^{S}P_M|m_s|^2}{\sigma^2}$, $\gamma_{x_\ell} = \frac{P_S|h_\ell|^2}{\sigma^2}$ and $\gamma_{x_L} = \sum_{\ell=1}^{i-1}\gamma_{x_\ell}$, $\gamma_C = \frac{P_R|c|^2}{\sigma^2}$, and $\Psi_1 = \gamma_y\left(\sum_{j=i+1}^{N-1}\beta_j\gamma_{x_J} + \sum_{k=1}^{K}\alpha_k\gamma_F + \sum_{\ell=1}^{i-1}\beta_\ell\gamma_{x_L}+1\right) + \beta_i\gamma_{x_i}\left(\sum_{s=1}^{S}\theta_s\gamma_M+1\right)$, $\Psi_2 = \sum_{s=1}^{S}\theta_s\gamma_M\sum_{j=i+1}^{N-1}\beta_j\gamma_{x_J} + \sum_{s=1}^{S}\theta_s\gamma_M\sum_{k=1}^{K}\alpha_k\gamma_F + \sum_{s=1}^{S}\theta_s\gamma_M + \sum_{j=i+1}^{N-1}\beta_j\gamma_{x_J} + \sum_{k=1}^{K}\alpha_k\gamma_F + 1$, $\Delta_1 = \gamma_y\left(\sum_{k=1}^{K}\alpha_k\gamma_F + \sum_{\ell=1}^{i-1}\beta_\ell\gamma_{x_L}+1\right) + \beta_N\gamma_{x_N}\left(\sum_{s=1}^{S}\theta_s\gamma_M+1\right)$, $\Delta_2 = \sum_{s=1}^{S}\theta_s\gamma_M\sum_{i=1}^{N-1}\beta_i\gamma_{x_i} + \sum_{s=1}^{S}\theta_s\gamma_M\sum_{k=1}^{K}\alpha_k\gamma_F + \sum_{s=1}^{S}\theta_s\gamma_M + \sum_{i=1}^{N-1}\beta_i\gamma_{x_i} + \sum_{k=1}^{K}\alpha_k\gamma_F + 1$, $\Lambda_1 = \gamma_y\left(\sum_{j=i+1}^{N-1}\beta_j\gamma_{x_J} + \sum_{k=1}^{K}\alpha_k\gamma_F + \gamma_C + \sum_{\ell=1}^{i-1}\beta_\ell\gamma_{x_L}+1\right) + \beta_i\gamma_{x_i}\left(\sum_{s=1}^{S}\theta_s\gamma_M+1\right)$, $\Lambda_2 = \sum_{s=1}^{S}\theta_s\gamma_M\sum_{j=i+1}^{N-1}\beta_j\gamma_{x_J} + \sum_{s=1}^{S}\theta_s\gamma_M\sum_{k=1}^{K}\alpha_k\gamma_F + \sum_{s=1}^{S}\theta_s\gamma_M + \gamma_C + \sum_{s=1}^{S}\theta_s\gamma_M + \sum_{j=i+1}^{N-1}\beta_j\gamma_{x_J} + \sum_{k=1}^{K}\alpha_k\gamma_F + \gamma_C + 1$, $\Upsilon_1 = \gamma_y\left(\sum_{k=1}^{K}\alpha_k\gamma_F + \gamma_C + \sum_{\ell=1}^{i-1}\beta_\ell\gamma_{x_L}+1\right) + \beta_N\gamma_{x_N}\left(\sum_{s=1}^{S}\theta_s\gamma_M+1\right)$, $\Upsilon_2 = \sum_{s=1}^{S}\theta_s\gamma_M\sum_{i=1}^{N-1}\beta_i\gamma_{x_i} + \sum_{s=1}^{S}\theta_s\gamma_M\sum_{k=1}^{K}\alpha_k\gamma_F + \sum_{s=1}^{S}\theta_s\gamma_M\gamma_C + \sum_{s=1}^{S}\theta_s\gamma_M + \sum_{i=1}^{N-1}\beta_i\gamma_{x_i} + \sum_{k=1}^{K}\alpha_k\gamma_F + \gamma_C + 1$.

III. THEORETICAL ANALYSIS

This section provides the analytical expressions of the outage probability, error probability, throughput, spectral and energy efficiencies.

A. OUTAGE PROBABILITY ANALYSIS

The outage probability (OP) event for user U_i is defined as the probability that the pre-defined target rate for the i-th user $R_{th,i}$ in bps/Hz, cannot be supported. The outage probability can also be defined as the CDF of received signal-to-noise ratio (SNR)/signal-to-interference noise ratio (SINR), evaluated at the target threshold rate for HD and FD modes, $\gamma_{th,i}^{HD} \equiv 2^{2R_{th,i}} - 1$ [48], [49] and $\gamma_{th,i}^{FD} \equiv 2^{R_{th,i}} - 1$ [50], respectively. In this context, given the intractable form of the SINR expressions stemming from (9), (10), (11), and (12), it is feasible to establish upper-bounds for these expressions as

$$\gamma_{x_i}^{\mathrm{HD}} = \frac{\frac{\beta_i\gamma_{x_i}\gamma_y}{\left(\sum_{j=i+1}^{N-1}\beta_j\gamma_{x_J}+\delta\right)\left(\sum_{s=1}^{S}\theta_s\gamma_M+1\right)}}{\frac{\beta_i\gamma_{x_i}}{\left(\sum_{j=i+1}^{N-1}\beta_j\gamma_{x_J}+\delta\right)} + \frac{\gamma_y}{\left(\sum_{s=1}^{S}\theta_s\gamma_M+1\right)} + \Psi_2} = \beta_i\frac{A_1B_1}{A_1+B_1} \le \gamma_{x_i}^{\mathrm{HD,up}} = \beta_i\min(\mathrm{A}_1, \mathrm{B}_1), \quad (17)$$

$$\gamma_{x_N}^{\mathrm{HD}} = \frac{\frac{\beta_N\gamma_{x_N}\gamma_y}{(\delta)\left(\sum_{s=1}^{S}\theta_s\gamma_M+1\right)}}{\frac{\beta_N\gamma_{x_N}}{(\delta)} + \frac{\gamma_y}{\left(\sum_{s=1}^{S}\theta_s\gamma_M+1\right)} + \Delta_2} = \beta_N\frac{C_1D_1}{C_1+D_1} \le \gamma_{x_N}^{\mathrm{HD,up}} = \beta_N\min(\mathrm{C}_1, \mathrm{D}_1), \quad (18)$$

$$\gamma_{x_i}^{\mathrm{FD}} = \frac{\frac{\beta_i\gamma_{x_i}\gamma_y}{\left(\sum_{j=i+1}^{N-1}\beta_j\gamma_{x_J}+\gamma_C+\delta\right)\left(\sum_{s=1}^{S}\theta_s\gamma_M+1\right)}}{\frac{\beta_i\gamma_{x_i}}{\left(\sum_{j=i+1}^{N-1}\beta_j\gamma_{x_J}+\gamma_C+\delta\right)} + \frac{\gamma_y}{\left(\sum_{s=1}^{S}\theta_s\gamma_M+1\right)} + \Lambda_2} = \beta_i\frac{E_1F_1}{E_1+F_1} \le \gamma_{x_i}^{\mathrm{FD,up}} = \beta_i\min(\mathrm{E}_1, \mathrm{F}_1), \quad (19)$$

$$\gamma_{x_N}^{\mathrm{FD}} = \frac{\frac{\beta_N\gamma_{x_N}\gamma_y}{(\gamma_C+\delta)\left(\sum_{s=1}^{S}\theta_s\gamma_M+1\right)}}{\frac{\beta_N\gamma_{x_N}}{(\gamma_C+\delta)} + \frac{\gamma_y}{\left(\sum_{s=1}^{S}\theta_s\gamma_M+1\right)} + \Upsilon_2} = \beta_N\frac{G_1H_1}{G_1+H_1} \le \gamma_{x_N}^{\mathrm{FD,up}} = \beta_N\min(\mathrm{G}_1, \mathrm{H}_1), \quad (20)$$

where $\delta = \sum_{k=1}^{K} \alpha_k \gamma_F + \sum_{\ell=1}^{i-1} \beta_\ell \gamma_{x_L} + 1$, $A_1 = \frac{\gamma_{x_i}}{\left(\sum_{j=i+1}^{N-1} \beta_j \gamma_{x_J} + \sum_{k=1}^{K} \alpha_k \gamma_F + \sum_{\ell=1}^{i-1} \beta_\ell \gamma_{x_L} + 1\right)}$, $B_1 = \frac{\gamma_y}{\left(\sum_{s=1}^{S} \theta_s \gamma_M + 1\right)}$, $C_1 = \frac{\gamma_{x_N}}{\left(\sum_{k=1}^{K} \alpha_k \gamma_F + \sum_{\ell=1}^{i-1} \beta_\ell \gamma_{x_L} + 1\right)}$, and $D_1 = \frac{\gamma_y}{\left(\sum_{s=1}^{S} \theta_s \gamma_M + 1\right)}$, $E_1 = \frac{\gamma_{x_i}}{\left(\sum_{j=i+1}^{N-1} \beta_j \gamma_{x_J} + \sum_{k=1}^{K} \alpha_k \gamma_F + \gamma_C + \sum_{\ell=1}^{i-1} \beta_\ell \gamma_{x_L} + 1\right)}$, $F_1 = \frac{\gamma_y}{\left(\sum_{s=1}^{S} \theta_s \gamma_M + 1\right)}$, $G_1 = \frac{\gamma_{x_N}}{\left(\sum_{k=1}^{K} \alpha_k \gamma_F + \gamma_C + \sum_{\ell=1}^{i-1} \beta_\ell \gamma_{x_L} + 1\right)}$, and $H_1 = \frac{\gamma_y}{\left(\sum_{s=1}^{S} \theta_s \gamma_M + 1\right)}$.

Proposition 1: The outage probability expressions for U_i and U_N for HD and FD modes along with non-orthogonal CCI are obtained as in (21), (22), (23), and (24).

$$\begin{aligned}
&\mathsf{P}_{\text{out}}^{\text{up,i,HD}}\left(\gamma_{\text{th,i}}^{\text{HD}}\right) \\
&= 1 - \left(\frac{1}{\mathrm{P}_s \Omega_{h_j}}\right)^{N-1} \left(\frac{1}{\mathrm{P}_s \Omega_{h_j}} + \frac{\sum_{j=i+1}^{N-1} \beta_j \gamma_{\text{th,i}}^{\text{HD}}}{P_S \Omega_{h_i} \beta_i}\right)^{1-N} \\
&\times \left(\frac{1}{P_F \Omega_{f_k}}\right)^{K} \left(\frac{1}{P_F \Omega_{f_k}} + \frac{\sum_{k=1}^{K} \alpha_k \gamma_{\text{th,i}}^{\text{HD}}}{P_S \Omega_{h_i} \beta_i}\right)^{-K} \\
&\times \left(\frac{1}{P_s \Omega_{h_\ell}}\right)^{i-1} \left(\frac{1}{P_s \Omega_{h_\ell}} + \frac{\sum_{\ell=1}^{i-1} \beta_\ell \gamma_{\text{th,i}}^{\text{HD}}}{P_S \Omega_{h_i} \beta_i}\right)^{1-i} \left(\frac{1}{P_M \Omega_{m_s}}\right)^{S} \\
&\times \left(\frac{1}{P_M \Omega_{m_s}} + \frac{\sum_{s=1}^{S} \theta_s \gamma_{\text{th,i}}^{\text{HD}}}{P_R \Omega_g \beta_i}\right)^{-S} e^{-\gamma_{\text{th,i}}^{\text{HD}} \left(\frac{1}{P_S \Omega_{h_i} \beta_i} + \frac{1}{P_R \Omega_g \beta_i}\right)}, \quad (21)
\end{aligned}$$

$$\begin{aligned}
&\mathsf{P}_{\text{out}}^{\text{up,N,HD}}\left(\gamma_{\text{th,N}}^{\text{HD}}\right) \\
&= 1 - \left(\frac{1}{P_F \Omega_{f_k}}\right)^{K} \left(\frac{1}{P_F \Omega_{f_k}} + \frac{\sum_{k=1}^{K} \alpha_k \gamma_{\text{th,N}}^{\text{HD}}}{P_S \Omega_{h_N} \beta_N}\right)^{-K} \\
&\times \left(\frac{1}{P_s \Omega_{h_\ell}}\right)^{N-1} \left(\frac{1}{P_s \Omega_{h_\ell}} + \frac{\sum_{\ell=1}^{N-1} \beta_\ell \gamma_{\text{th,N}}^{\text{HD}}}{P_S \Omega_{h_N} \beta_N}\right)^{1-N} \\
&\times \left(\frac{1}{P_M \Omega_{m_s}}\right)^{S} \left(\frac{1}{P_M \Omega_{m_s}} + \frac{\sum_{s=1}^{S} \theta_s \gamma_{\text{th,N}}^{\text{HD}}}{P_R \Omega_g \beta_N}\right)^{-S} \\
&\times e^{-\gamma_{\text{th,N}}^{\text{HD}} \left(\frac{1}{P_S \Omega_{h_N} \beta_N} + \frac{1}{P_R \Omega_g \beta_N}\right)}, \quad (22)
\end{aligned}$$

$$\begin{aligned}
&\mathsf{P}_{\text{out}}^{\text{up,i,FD}}\left(\gamma_{\text{th,i}}^{\text{FD}}\right) \\
&= 1 - \left(\frac{1}{\mathrm{P}_s \Omega_{h_j}}\right)^{N-1} \left(\frac{1}{\mathrm{P}_s \Omega_{h_j}} + \frac{\sum_{j=i+1}^{N-1} \beta_j \gamma_{\text{th,i}}^{\text{FD}}}{P_S \Omega_{h_i} \beta_i}\right)^{1-N} \\
&\times \left(\frac{1}{P_F \Omega_{f_k}}\right)^{K} \left(\frac{1}{P_F \Omega_{f_k}} + \frac{\sum_{k=1}^{K} \alpha_k \gamma_{\text{th,i}}^{\text{FD}}}{P_S \Omega_{h_i} \beta_i}\right)^{-K} \\
&\times \left(\frac{1}{P_R \Omega_c}\right) \left(\frac{1}{P_R \Omega_c} + \frac{\gamma_{\text{th,i}}^{\text{FD}}}{P_S \Omega_{h_i} \beta_i}\right)^{-1} \left(\frac{1}{P_s \Omega_{h_\ell}}\right)^{i-1} \\
&\times \left(\frac{1}{P_s \Omega_{h_\ell}} + \frac{\sum_{\ell=1}^{i-1} \beta_\ell \gamma_{\text{th,i}}^{\text{FD}}}{P_S \Omega_{h_i} \beta_i}\right)^{1-i} \left(\frac{1}{P_M \Omega_{m_s}}\right)^{S} \\
&\times \left(\frac{1}{P_M \Omega_{m_s}} + \frac{\sum_{s=1}^{S} \theta_s \gamma_{\text{th,i}}^{\text{FD}}}{P_R \Omega_g \beta_i}\right)^{-S} \\
&\times e^{-\gamma_{\text{th,i}}^{\text{FD}} \left(\frac{1}{P_S \Omega_{h_i} \beta_i} + \frac{1}{P_R \Omega_g \beta_i}\right)}, \quad (23)
\end{aligned}$$

$$\begin{aligned}
&\mathsf{P}_{\text{out}}^{\text{up,N,FD}}\left(\gamma_{\text{th,N}}^{\text{FD}}\right) \\
&= 1 - \left(\frac{1}{P_F \Omega_{f_k}}\right)^{K} \left(\frac{1}{P_F \Omega_{f_k}} + \frac{\sum_{k=1}^{K} \alpha_k \gamma_{\text{th,N}}^{\text{FD}}}{P_S \Omega_{h_N} \beta_N}\right)^{-K} \\
&\times \left(\frac{1}{P_R \Omega_c}\right) \left(\frac{1}{P_R \Omega_c} + \frac{\gamma_{\text{th,N}}^{\text{FD}}}{P_S \Omega_{h_N} \beta_N}\right)^{-1} \\
&\times \left(\frac{1}{P_s \Omega_{h_\ell}}\right)^{N-1} \left(\frac{1}{P_s \Omega_{h_\ell}} + \frac{\sum_{\ell=1}^{N-1} \beta_\ell \gamma_{\text{th,N}}^{\text{FD}}}{P_S \Omega_{h_N} \beta_N}\right)^{1-N} \\
&\times \left(\frac{1}{P_M \Omega_{m_s}}\right)^{S} \left(\frac{1}{P_M \Omega_{m_s}} + \frac{\sum_{s=1}^{S} \theta_s \gamma_{\text{th,N}}^{\text{FD}}}{P_R \Omega_g \beta_N}\right)^{-S} \\
&\times e^{-\gamma_{\text{th,N}}^{\text{FD}} \left(\frac{1}{P_S \Omega_{h_N} \beta_N} + \frac{1}{P_R \Omega_g \beta_N}\right)}. \quad (24)
\end{aligned}$$

Proof: See Appendix. ■

B. ERROR PROBABILITY

Error Probability is a crucial performance metric for the information exchange process in wireless networks. Utilizing [51], the CDF-based EP performance metric is written

$$\bar{\mathsf{P}}_{\mathsf{e}} = \frac{a}{2}\sqrt{\frac{b}{\pi}} \int_0^{\infty} \frac{\exp(-\mathrm{b}x)}{\sqrt{x}} F(x) dx, \quad (25)$$

where $a = b = 1$ represents the BPSK and $a = b = 2$ represents the QPSK modulations. BPSK modulation is considered for the performance analysis. Related analytical derivations are presented as in the Proposition 2.

Proposition 2: The EP expressions for the i-th and N-th users along with HD and FD modes are expressed as in (26), (27), (28), and (29), shown on the next page, where $\Phi_2 = \frac{1}{\mathrm{P}_s \Omega_{\mathrm{h_i}} \beta_{\mathrm{i}}} + \frac{1}{P_R \Omega_g \beta_i} + 1$ and $\Phi_3 = \frac{1}{\mathrm{P}_s \Omega_{\mathrm{h_N}} \beta_{\mathrm{N}}} + \frac{1}{P_R \Omega_g \beta_N} + 1$.

Proof: See Appendix. ■

C. THROUGHPUT ANALYSIS

The throughput expressions for the HD and FD relay-aided uplink NOMA network in the presence of non-orthogonal CCI can be obtained by considering [52, Eq. (15(a))] and the outage expressions from Proposition 1, first,

$$\mathsf{P_e}^{\mathrm{i,HD}} = 0.5 - \frac{1}{2\sqrt{\pi}}(\Phi_2)^{-1/2}\left(\frac{\sum_{a=1}^{K} A_a}{\Gamma(N-1)\Gamma(a)} G_{1,0:1,1:1,1}^{1,0:1,1:1,1}\left(\begin{matrix}0.5 \\ -\end{matrix}\middle|\begin{matrix}2-N \\ 0\end{matrix}\middle|\begin{matrix}1-a \\ 0\end{matrix}\middle|\frac{\frac{\mathrm{P_s}\Omega_{\mathrm{h_j}}\sum_{\mathrm{j=i+1}}^{\mathrm{N-1}}\beta_{\mathrm{j}}}{\mathrm{P_s}\Omega_{\mathrm{h_i}}\beta_{\mathrm{i}}}}{\Phi_2}, \frac{\frac{\sum_{k=1}^{K}\alpha_k P_F \Omega_{f_k}}{\mathrm{P_s}\Omega_{\mathrm{h_i}}\beta_{\mathrm{i}}}}{\Phi_2}\right)\right.$$
$$+ \frac{\sum_{b=1}^{i-1} B_b}{\Gamma(N-1)\Gamma(b)} G_{1,0:1,1:1,1}^{1,0:1,1:1,1}\left(\begin{matrix}0.5 \\ -\end{matrix}\middle|\begin{matrix}2-N \\ 0\end{matrix}\middle|\begin{matrix}1-b \\ 0\end{matrix}\middle|\frac{\frac{\mathrm{P_s}\Omega_{\mathrm{h_j}}\sum_{\mathrm{j=i+1}}^{\mathrm{N-1}}\beta_{\mathrm{j}}}{\mathrm{P_s}\Omega_{\mathrm{h_i}}\beta_{\mathrm{i}}}}{\Phi_2}, \frac{\frac{\sum_{\ell=1}^{i-1}\beta_\ell \mathrm{P_s}\Omega_{\mathrm{h}_\ell}}{\mathrm{P_s}\Omega_{\mathrm{h_i}}\beta_{\mathrm{i}}}}{\Phi_2}\right)$$
$$\left. + \frac{\sum_{c=1}^{S} C_c}{\Gamma(N-1)\Gamma(c)} G_{1,0:1,1:1,1}^{1,0:1,1:1,1}\left(\begin{matrix}0.5 \\ -\end{matrix}\middle|\begin{matrix}2-N \\ 0\end{matrix}\middle|\begin{matrix}1-c \\ 0\end{matrix}\middle|\frac{\frac{\mathrm{P_s}\Omega_{\mathrm{h_j}}\sum_{\mathrm{j=i+1}}^{\mathrm{N-1}}\beta_{\mathrm{j}}}{\mathrm{P_s}\Omega_{\mathrm{h_i}}\beta_{\mathrm{i}}}}{\Phi_2}, \frac{\frac{\sum_{s=1}^{S}\theta_s P_M \Omega_{m_s}}{P_R\Omega_g\beta_i}}{\Phi_2}\right)\right) \tag{26}$$

$$\mathsf{P_e}^{\mathrm{N,HD}} = 0.5 - \frac{1}{2\sqrt{\pi}}(\Phi_3)^{-1/2}\left(\frac{\sum_{d=1}^{K} D_d}{\Gamma(N-1)\Gamma(d)} G_{1,0:1,1:1,1}^{1,0:1,1:1,1}\left(\begin{matrix}0.5 \\ -\end{matrix}\middle|\begin{matrix}2-N \\ 0\end{matrix}\middle|\begin{matrix}1-d \\ 0\end{matrix}\middle|\frac{\frac{\sum_{\ell=1}^{N-1}\beta_\ell \mathrm{P_s}\Omega_{\mathrm{h}_\ell}}{\mathrm{P_s}\Omega_{\mathrm{h_N}}\beta_{\mathrm{N}}}}{\Phi_3}, \frac{\frac{\sum_{k=1}^{K}\alpha_k P_F \Omega_{f_k}}{\mathrm{P_s}\Omega_{\mathrm{h_N}}\beta_{\mathrm{N}}}}{\Phi_3}\right)\right.$$
$$\left. + \frac{\sum_{e=1}^{S} E_e}{\Gamma(N-1)\Gamma(e)} G_{1,0:1,1:1,1}^{1,0:1,1:1,1}\left(\begin{matrix}0.5 \\ -\end{matrix}\middle|\begin{matrix}2-N \\ 0\end{matrix}\middle|\begin{matrix}1-e \\ 0\end{matrix}\middle|\frac{\frac{\sum_{\ell=1}^{N-1}\beta_\ell \mathrm{P_s}\Omega_{\mathrm{h}_\ell}}{\mathrm{P_s}\Omega_{\mathrm{h_N}}\beta_{\mathrm{N}}}}{\Phi_3}, \frac{\frac{\sum_{s=1}^{S}\theta_s P_M \Omega_{m_s}}{P_R\Omega_g\beta_N}}{\Phi_3}\right)\right. \tag{27}$$

$$\mathsf{P_e}^{\mathrm{i,FD}} = 0.5 - \frac{1}{2\sqrt{\pi}}(\Phi_2)^{-1/2}\left(\frac{\sum_{f=1}^{K} F_f}{\Gamma(N-1)\Gamma(f)} G_{1,0:1,1:1,1}^{1,0:1,1:1,1}\left(\begin{matrix}0.5 \\ -\end{matrix}\middle|\begin{matrix}2-N \\ 0\end{matrix}\middle|\begin{matrix}1-f \\ 0\end{matrix}\middle|\frac{\frac{\mathrm{P_s}\Omega_{\mathrm{h_j}}\sum_{\mathrm{j=i+1}}^{\mathrm{N-1}}\beta_{\mathrm{j}}}{\mathrm{P_s}\Omega_{\mathrm{h_i}}\beta_{\mathrm{i}}}}{\Phi_2}, \frac{\frac{\sum_{k=1}^{K}\alpha_k P_F \Omega_{f_k}}{\mathrm{P_s}\Omega_{\mathrm{h_i}}\beta_{\mathrm{i}}}}{\Phi_2}\right)\right.$$
$$+ \frac{\sum_{g=1}^{1-i} G_g}{\Gamma(N-1)\Gamma(g)} G_{1,0:1,1:1,1}^{1,0:1,1:1,1}\left(\begin{matrix}0.5 \\ -\end{matrix}\middle|\begin{matrix}2-N \\ 0\end{matrix}\middle|\begin{matrix}1-g \\ 0\end{matrix}\middle|\frac{\frac{\mathrm{P_s}\Omega_{\mathrm{h_j}}\sum_{\mathrm{j=i+1}}^{\mathrm{N-1}}\beta_{\mathrm{j}}}{\mathrm{P_s}\Omega_{\mathrm{h_i}}\beta_{\mathrm{i}}}}{\Phi_2}, \frac{\frac{\sum_{\ell=1}^{i-1}\beta_\ell \mathrm{P_s}\Omega_{\mathrm{h}_\ell}}{\mathrm{P_s}\Omega_{\mathrm{h_i}}\beta_{\mathrm{i}}}}{\Phi_2}\right)$$
$$\left. + \frac{H}{\Gamma(N-1)} G_{1,0:1,1:1,1}^{1,0:1,1:1,1}\left(\begin{matrix}0.5 \\ -\end{matrix}\middle|\begin{matrix}2-N \\ 0\end{matrix}\middle|\begin{matrix}0 \\ 0\end{matrix}\middle|\frac{\frac{\mathrm{P_s}\Omega_{\mathrm{h_j}}\sum_{\mathrm{j=i+1}}^{\mathrm{N-1}}\beta_{\mathrm{j}}}{\mathrm{P_s}\Omega_{\mathrm{h_i}}\beta_{\mathrm{i}}}}{\Phi_2}, \frac{\frac{P_R\Omega_c}{\mathrm{P_s}\Omega_{\mathrm{h_i}}\beta_{\mathrm{i}}}}{\Phi_2}\right)\right)$$
$$+ \frac{\sum_{t=1}^{S} T_t}{\Gamma(N-1)\Gamma(t)} G_{1,0:1,1:1,1}^{1,0:1,1:1,1}\left(\begin{matrix}0.5 \\ -\end{matrix}\middle|\begin{matrix}2-N \\ 0\end{matrix}\middle|\begin{matrix}1-t \\ 0\end{matrix}\middle|\frac{\frac{\mathrm{P_s}\Omega_{\mathrm{h_j}}\sum_{\mathrm{j=i+1}}^{\mathrm{N-1}}\beta_{\mathrm{j}}}{\mathrm{P_s}\Omega_{\mathrm{h_i}}\beta_{\mathrm{i}}}}{\Phi_2}, \frac{\frac{\sum_{s=1}^{S}\theta_s P_M \Omega_{m_s}}{P_R\Omega_g\beta_i}}{\Phi_2}\right) \tag{28}$$

$$\mathsf{P_e}^{\mathrm{N,FD}} = 0.5 - \frac{1}{2\sqrt{\pi}}(\Phi_3)^{-1/2}\left(\frac{\sum_{o=1}^{K} O_o}{\Gamma(N-1)\Gamma(o)} G_{1,0:1,1:1,1}^{1,0:1,1:1,1}\left(\begin{matrix}0.5 \\ -\end{matrix}\middle|\begin{matrix}2-N \\ 0\end{matrix}\middle|\begin{matrix}1-o \\ 0\end{matrix}\middle|\frac{\frac{\mathrm{P_s}\Omega_{\mathrm{h}_\ell}\sum_{\ell=1}^{\mathrm{N-1}}\beta_\ell}{\mathrm{P_s}\Omega_{\mathrm{h_N}}\beta_{\mathrm{N}}}}{\Phi_3}, \frac{\frac{\sum_{k=1}^{K}\alpha_k P_F \Omega_{f_k}}{\mathrm{P_s}\Omega_{\mathrm{h_N}}\beta_N}}{\Phi_3}\right)\right.$$
$$+ \frac{P}{\Gamma(N-1)} G_{1,0:1,1:1,1}^{1,0:1,1:1,1}\left(\begin{matrix}0.5 \\ -\end{matrix}\middle|\begin{matrix}2-N \\ 0\end{matrix}\middle|\begin{matrix}0 \\ 0\end{matrix}\middle|\frac{\frac{\mathrm{P_s}\Omega_{\mathrm{h}_\ell}\sum_{\ell=1}^{\mathrm{N-1}}\beta_\ell}{\mathrm{P_s}\Omega_{\mathrm{h_N}}\beta_{\mathrm{N}}}}{\Phi_3}, \frac{\frac{P_R\Omega_c}{\mathrm{P_s}\Omega_{\mathrm{h_N}}\beta_{\mathrm{N}}}}{\Phi_3}\right)$$
$$\left. + \frac{\sum_{r=1}^{S} R_r}{\Gamma(N-1)\Gamma(r)} G_{1,0:1,1:1,1}^{1,0:1,1:1,1}\left(\begin{matrix}0.5 \\ -\end{matrix}\middle|\begin{matrix}2-N \\ 0\end{matrix}\middle|\begin{matrix}1-r \\ 0\end{matrix}\middle|\frac{\frac{\mathrm{P_s}\Omega_{\mathrm{h}_\ell}\sum_{\ell=1}^{\mathrm{N-1}}\beta_\ell}{\mathrm{P_s}\Omega_{\mathrm{h_N}}\beta_{\mathrm{N}}}}{\Phi_3}, \frac{\frac{\sum_{s=1}^{S}\theta_s P_M \Omega_{m_s}}{P_R\Omega_g\beta_N}}{\Phi_3}\right)\right. \tag{29}$$

for the HD mode as

$$\tau^{\mathrm{up,i,HD}} = \frac{1}{2} R_{th,i}^{HD} \left(1 - \mathsf{P}_{\mathsf{out}}^{\mathrm{up,i,HD}}(\gamma_{\mathrm{th,i}}^{\mathrm{HD}})\right), \tag{30}$$

$$\tau^{\mathrm{up,N,HD}} = \frac{1}{2} R_{th,N}^{HD} \left(1 - \mathsf{P}_{\mathsf{out}}^{\mathrm{up,N,HD}}(\gamma_{\mathrm{th,N}}^{\mathrm{HD}})\right), \tag{31}$$

and then, for the FD mode as

$$\tau^{\mathrm{up,i,FD}} = R_{th,i}^{FD} \left(1 - \mathsf{P}_{\mathsf{out}}^{\mathrm{up,i,FD}}(\gamma_{\mathrm{th,i}}^{\mathrm{FD}})\right), \tag{32}$$

$$\tau^{\mathrm{up,N,FD}} = R_{th,N}^{FD} \left(1 - \mathsf{P}_{\mathsf{out}}^{\mathrm{up,N,FD}}(\gamma_{\mathrm{th,N}}^{\mathrm{FD}})\right). \tag{33}$$

D. SPECTRAL EFFICIENCY ANALYSIS

To evaluate the system performance, we consider the sum spectral efficiency (SE), which is defined as the sum-rate (in bits) per channel use [53]. In this regard, utilizing (30)–(33), the SE for the HD and FD modes is formulated as

$$\mathsf{SE}^{\mathsf{HD/FD}} = \sum_{i=1}^{N} \tau^{\mathrm{i,HD/FD}}. \tag{34}$$

E. ENERGY EFFICIENCY ANALYSIS

The energy efficiency (EE) (in bits/Joule) is a key performance metric for wireless communication networks, which is defined as the sum SE divided by the total transmit power [53]. Therefore, by using the SE expression in (33), the EE for the HD/FD modes are obtained as

$$\mathsf{EE}^{\mathsf{HD}} = \frac{\sum_{i=1}^{N} \tau^{\mathrm{i,HD}}}{\sum_{i=1}^{N} P_i + P_R}, \tag{35}$$

and for the FD mode as

$$\mathsf{EE}^{\mathsf{FD}} = \frac{\sum_{i=1}^{N} \tau^{\mathrm{i,FD}}}{\sum_{i=1}^{N} P_i + P_R}. \tag{36}$$

IV. ASYMPTOTIC ANALYSIS

This section provides a deeper insight on the derived analytical results. The asymptotic expressions of the outage and error probabilities are presented in the following paragraphs, while the other performance metrics' asymptotic derivations are omitted for brevity. However, they are evaluated in the numerical results section. In order to provide further insights on the outage, error, throughput, and energy efficiency performance, their asymptotic expressions can be obtained by utilizing $\exp(-\mathrm{x}) \approx 1 - \mathrm{x}$, $x \to 0$, and the approximation $(1+x)^{-K} \approx (1 - Kx)$ [54].

A. OUTAGE PROBABILITY

The outage probability asymptotic expressions for i-th and N-th users for the HD and FD modes are presented as in (37), (38), (39), and (40), shown at the bottom of the page, respectively.

$$\bar{\mathsf{P}}_{\mathsf{out}}^{\mathrm{up,i,HD},\infty}(\gamma_{\mathrm{th,i}}^{\mathrm{HD}}) = 1 - \left(1 + (1-N)\frac{\gamma_{\mathrm{th,i}}^{\mathrm{HD}} \mathrm{P_s}\Omega_{\mathrm{h_j}} \sum_{\mathrm{j=i+1}}^{\mathrm{N-1}} \beta_{\mathrm{j}}}{P_S \Omega_{h_i} \beta_i}\right)\left(1 - K\frac{P_F \Omega_{f_k} \sum_{k=1}^{K} \alpha_k \gamma_{\mathrm{th,i}}^{\mathrm{HD}}}{P_S \Omega_{h_i} \beta_i}\right)$$
$$\times \left(1 + (1-i)\frac{P_s \Omega_{h_\ell} \sum_{\ell=1}^{i-1} \beta_\ell \gamma_{\mathrm{th,i}}^{\mathrm{HD}}}{P_S \Omega_{h_i} \beta_i}\right)\left(1 - S\frac{P_M \Omega_{m_s} \sum_{s=1}^{S} \theta_s \gamma_{\mathrm{th,i}}^{\mathrm{HD}}}{P_R \Omega_g \beta_i}\right)\left(1 - \gamma_{\mathrm{th,i}}^{\mathrm{HD}}\left(\frac{1}{P_S \Omega_{h_i} \beta_i} + \frac{1}{P_R \Omega_g \beta_i}\right)\right), \tag{37}$$

$$\mathsf{P}_{\mathsf{out}}^{\mathrm{up,N,HD},\infty}(\gamma_{\mathrm{th,N}}^{\mathrm{HD}}) = 1 - \left(1 - K\frac{P_F \Omega_{f_k} \sum_{k=1}^{K} \alpha_k \gamma_{\mathrm{th,N}}^{\mathrm{HD}}}{P_S \Omega_{h_N} \beta_N}\right)\left(1 + (1-N)\frac{P_s \Omega_{h_\ell} \sum_{\ell=1}^{N-1} \beta_\ell \gamma_{\mathrm{th,N}}^{\mathrm{HD}}}{P_S \Omega_{h_N} \beta_N}\right)$$
$$\times \left(1 - S\frac{P_M \Omega_{m_s} \sum_{s=1}^{S} \theta_s \gamma_{\mathrm{th,N}}^{\mathrm{HD}}}{P_R \Omega_g \beta_N}\right)\left(1 - \gamma_{\mathrm{th,N}}^{\mathrm{HD}}\left(\frac{1}{P_S \Omega_{h_N} \beta_N} + \frac{1}{P_R \Omega_g \beta_N}\right)\right), \tag{38}$$

$$\mathsf{P}_{\mathsf{out}}^{\mathrm{up,i,FD},\infty}(\gamma_{\mathrm{th,i}}^{\mathrm{FD}}) = 1 - \left(1 + (1-N)\frac{\mathrm{P_s}\Omega_{\mathrm{h_j}} \sum_{\mathrm{j=i+1}}^{\mathrm{N-1}} \beta_{\mathrm{j}} \gamma_{\mathrm{th,i}}^{\mathrm{FD}}}{P_S \Omega_{h_i} \beta_i}\right)\left(1 - K\frac{P_F \Omega_{f_k} \sum_{k=1}^{K} \alpha_k \gamma_{\mathrm{th,i}}^{\mathrm{FD}}}{P_S \Omega_{h_i} \beta_i}\right)\left(1 - \frac{P_R \Omega_c \gamma_{\mathrm{th,i}}^{\mathrm{FD}}}{P_S \Omega_{h_i} \beta_i}\right)$$
$$\times \left(1 + (1-i)\frac{\mathrm{P_s}\Omega_{\mathrm{h_\ell}} \sum_{\ell=1}^{\mathrm{i-1}} \beta_\ell \gamma_{\mathrm{th,i}}^{\mathrm{FD}}}{P_S \Omega_{h_i} \beta_i}\right)\left(1 - S\frac{P_M \Omega_{m_s} \sum_{s=1}^{S} \theta_s \gamma_{\mathrm{th,i}}^{\mathrm{FD}}}{P_R \Omega_g \beta_i}\right)\left(1 - \gamma_{\mathrm{th,i}}^{\mathrm{FD}}\left(\frac{1}{P_S \Omega_{h_i} \beta_i} + \frac{1}{P_R \Omega_g \beta_i}\right)\right), \tag{39}$$

$$\mathsf{P}_{\mathsf{out}}^{\mathrm{up,N,FD},\infty}(\gamma_{\mathrm{th,N}}^{\mathrm{FD}}) = 1 - \left(1 - K\frac{P_F \Omega_{f_k} \sum_{k=1}^{K} \alpha_k \gamma_{\mathrm{th,N}}^{\mathrm{FD}}}{P_S \Omega_{h_N} \beta_N}\right)\left(1 - \frac{P_R \Omega_c \gamma_{\mathrm{th,N}}^{\mathrm{FD}}}{P_S \Omega_{h_N} \beta_N}\right)\left(1 + (1-N)\frac{P_s \Omega_{h_\ell} \sum_{\ell=1}^{N-1} \beta_\ell \gamma_{\mathrm{th,N}}^{\mathrm{FD}}}{P_S \Omega_{h_N} \beta_N}\right)$$
$$\times \left(1 - S\frac{P_M \Omega_{m_s} \sum_{s=1}^{S} \theta_s \gamma_{\mathrm{th,N}}^{\mathrm{FD}}}{P_R \Omega_g \beta_N}\right)\left(1 - \gamma_{\mathrm{th,N}}^{\mathrm{FD}}\left(\frac{1}{P_S \Omega_{h_N} \beta_N} + \frac{1}{P_R \Omega_g \beta_N}\right)\right). \tag{40}$$

B. ERROR PROBABILITY

The error probability asymptotic expressions for the i-th and N-th users for the HD and FD modes are presented as in (41), (42), (43), and (44), shown at the bottom of the page, the Proposition 3.

Proposition 3: Asymptotic EP expressions for the i-th and N-th users with the HD and FD modes are given as

Proof: See Appendix. ■

V. DIVERSITY ORDER ANALYSIS

The relation between the diversity order and the coding gain can be expressed as [55]

$$\overline{P}_{out} = (G_c\gamma)^{-G_d}, \tag{45}$$

where G_d is the diversity order and G_c is the coding gain. Interpreting the asymptotic CDF expression of $\bar{\mathrm{P}}_{\mathrm{out}}^{\mathrm{i,HD}}(\gamma_{\mathrm{th,i}}^{\mathrm{HD}})$, when P_S goes to infinity, the $\frac{P_F\Omega_{f_k}}{P_S\Omega_{h_i}\beta_i}$ term in $\left(1-\frac{K\gamma_{\mathrm{th,i}}^{HD}P_F\Omega_{f_k}}{P_S\Omega_{h_i}\beta_i}\right)$ becomes negligible and the $K\gamma_{\mathrm{th,i}}^{HD}$ term becomes dominant. When K increases, $\gamma_{th,i}^{HD}$ becomes negligible and the power of $\gamma_{th,i}^{HD}$, which is equal to zero, yields the diversity order. In addition, when P_R goes to infinity, the $\frac{P_M\Omega_{m_s}}{P_R\Omega_g\beta_i}$ term in $\left(1-\frac{S\gamma_{\mathrm{th,i}}^{HD}P_M\Omega_{m_s}}{P_R\Omega_g\beta_i}\right)$ becomes negligible and the $S\gamma_{\mathrm{th,i}}^{HD}$ term becomes dominant. When S increases, $\gamma_{\mathrm{th,i}}^{HD}$ becomes negligible and the power of $\gamma_{\mathrm{th,i}}^{HD}$, which is equal to zero, yields the diversity order. Following a similar approach, the N-th user's diversity order analysis in HD mode is obtained.

Regarding the diversity order, stemming from the asymptotic expression of $\bar{\mathrm{P}}_{\mathrm{out}}^{\mathrm{i,FD}}(\gamma_{\mathrm{th,i}}^{\mathrm{FD}})$, when P_S goes to infinity, the $\frac{P_F\Omega_{f_k}}{P_S\Omega_{h_i}\beta_i}$ term in $\left(1-\frac{K\gamma_{\mathrm{th,i}}^{FD}P_F\Omega_{f_k}}{P_S\Omega_{h_i}\beta_i}\right)$ becomes negligible and the $K\gamma_{\mathrm{th,i}}^{FD}$ term becomes dominant. When K increases, $\gamma_{\mathrm{th,i}}^{FD}$ becomes negligible and the power of $\gamma_{\mathrm{th,i}}^{FD}$, which is equal to zero, yields the diversity order. Likewise, when P_R goes to infinity, the $\frac{P_M\Omega_{m_s}}{P_R\Omega_g\beta_i}$ term in $\left(1-\frac{S\gamma_{\mathrm{th,i}}^{FD}P_M\Omega_{m_s}}{P_R\Omega_g\beta_i}\right)$ becomes negligible and $S\gamma_{\mathrm{th,i}}^{FD}$ becomes dominant. When S increases, $\gamma_{\mathrm{th,i}}^{FD}$ becomes negligible and the power of $\gamma_{\mathrm{th,i}}^{FD}$, which is equal to zero, yields the diversity order. In both scenarios, the system

$$\mathrm{P_e}^{\mathrm{i,HD},\infty} = 0.5 - \frac{1}{2\sqrt{\pi}}\left(\frac{1}{\mathrm{P_s}\Omega_{\mathrm{h_i}}\beta_{\mathrm{i}}} + \frac{1}{P_R\Omega_g\beta_i} + 1\right)^{-1/2}\left[\frac{\sum_{a=1}^{K} A_a\sqrt{\pi}\Gamma(a-0.5)}{\Gamma(N-1)\Gamma(a)}\left(\frac{\sum_{k=1}^{K}\alpha_k P_F\Omega_{f_k}}{\mathrm{P_s}\Omega_{\mathrm{h_i}}\beta_{\mathrm{i}}}\right)^{1/2}\right.$$
$$\left. + \frac{\sum_{b=1}^{i-1} B_b\sqrt{\pi}\Gamma(b-0.5)}{\Gamma(N-1)\Gamma(b)}\left(\frac{\sum_{\ell=1}^{i-1}\beta_\ell P_s\Omega_{h_\ell}}{\mathrm{P_s}\Omega_{\mathrm{h_i}}\beta_{\mathrm{i}}}\right)^{1/2} + \frac{\sum_{c=1}^{S} C_c\sqrt{\pi}\Gamma(c-0.5)}{\Gamma(N-1)\Gamma(c)}\left(\frac{\sum_{s=1}^{S}\theta_s P_M\Omega_{m_s}}{P_R\Omega_g\beta_i}\right)^{1/2}\right] \tag{41}$$

$$\mathrm{P_e}^{\mathrm{N,HD},\infty} = 0.5 - \frac{1}{2\sqrt{\pi}}\left(\frac{1}{\mathrm{P_s}\Omega_{\mathrm{h_N}}\beta_{\mathrm{N}}} + \frac{1}{P_R\Omega_g\beta_N} + 1\right)^{-1/2}\left[\frac{\sum_{d=1}^{K} D_d\sqrt{\pi}\Gamma(d-0.5)}{\Gamma(N-1)\Gamma(d)}\left(\frac{\sum_{k=1}^{K}\alpha_k P_F\Omega_{f_k}}{\mathrm{P_s}\Omega_{\mathrm{h_N}}\beta_{\mathrm{N}}}\right)^{1/2}\right.$$
$$\left. + \frac{\sum_{e=1}^{S} E_e\sqrt{\pi}\Gamma(e-0.5)}{\Gamma(N-1)\Gamma(e)}\left(\frac{\sum_{e=1}^{S}\theta_s P_M\Omega_{m_s}}{P_R\Omega_g\beta_N}\right)^{1/2}\right] \tag{42}$$

$$\mathrm{P_e}^{\mathrm{i,FD},\infty} = 0.5 - \frac{1}{2\sqrt{\pi}}\left(\frac{1}{\mathrm{P_s}\Omega_{\mathrm{h_i}}\beta_{\mathrm{i}}} + \frac{1}{P_R\Omega_g\beta_i} + 1\right)^{-1/2}\left[\frac{\sum_{f=1}^{K} F_f\sqrt{\pi}\Gamma(f-0.5)}{\Gamma(N-1)\Gamma(f)}\left(\frac{\sum_{k=1}^{K}\alpha_k P_F\Omega_{f_k}}{\mathrm{P_s}\Omega_{\mathrm{h_i}}\beta_{\mathrm{i}}}\right)^{1/2}\right.$$
$$+ \frac{\sum_{g=1}^{i-1} G_g\sqrt{\pi}\Gamma(g-0.5)}{\Gamma(N-1)\Gamma(g)}\left(\frac{\sum_{\ell=1}^{i-1}\beta_\ell \mathrm{P_s}\Omega_{\mathrm{h}_\ell}}{\mathrm{P_s}\Omega_{\mathrm{h_i}}\beta_{\mathrm{i}}}\right)^{1/2} + \frac{H\pi}{\Gamma(N-1)}\left(\frac{P_R\Omega_c}{\mathrm{P_s}\Omega_{\mathrm{h_i}}\beta_{\mathrm{i}}}\right)^{1/2}$$
$$\left. + \frac{\sum_{t=1}^{S} T_t\sqrt{\pi}\Gamma(t-0.5)}{\Gamma(N-1)\Gamma(t)}\left(\frac{\sum_{s=1}^{S}\theta_s P_M\Omega_{m_s}}{P_R\Omega_g\beta_i}\right)^{1/2}\right] \tag{43}$$

$$\mathrm{P_e}^{\mathrm{N,FD},\infty} = 0.5 - \frac{1}{2\sqrt{\pi}}\left(\frac{1}{\mathrm{P_s}\Omega_{\mathrm{h_N}}\beta_{\mathrm{N}}} + \frac{1}{P_R\Omega_g\beta_N} + 1\right)^{-1/2}\left[\frac{\sum_{o=1}^{K} O_o\sqrt{\pi}\Gamma(o-0.5)}{\Gamma(N-1)\Gamma(o)}\left(\frac{\sum_{k=1}^{K}\alpha_k P_F\Omega_{f_k}}{\mathrm{P_s}\Omega_{\mathrm{h_N}}\beta_{\mathrm{N}}}\right)^{1/2}\right.$$
$$\left. + \frac{P\pi}{\Gamma(N-1)}\left(\frac{P_R\Omega_c}{\mathrm{P_s}\Omega_{\mathrm{h_N}}\beta_N}\right)^{1/2} + \frac{\sum_{r=1}^{S} R_r\sqrt{\pi}\Gamma(r-0.5)}{\Gamma(N-1)\Gamma(r)}\left(\frac{\sum_{s=1}^{S}\theta_s P_M\Omega_{m_s}}{P_R\Omega_g\beta_N}\right)^{1/2}\right] \tag{44}$$

is characterized by a diversity order equal to zero. Likewise, following a similar approach, the N-th user's diversity order analysis in FD mode is obtained.

VI. RELAY LOCATION & POWER ALLOCATION OPTIMIZATION

In this section, relay location optimization under fixed power allocation and NOMA power allocation optimization for fixed relay location are presented.

A. OPTIMIZED RELAY POSITION UNDER FIXED POWER ALLOCATION

First, the distances among network nodes are defined, i.e. the distance between $U_i \rightarrow$ and the relay as d_i^v, the distance from the relay towards the BS as $(1-d_i)^v$, the distance between U_N and the relay as d_N^v, and the distance from the relay to the BS as $(1-d_N)^v$. The optimization problem and its constraints can be written as

$$\begin{aligned} \underset{d_i, d_N}{\text{minimize}} \quad & \mathsf{P}_{\text{out}}^{\text{up,i,HD}}\left(\gamma_{\text{th,i}}^{\text{HD}}\right) \\ \text{subject to} \quad & N \times P_S + P_R = P_T \text{ and } P_S > 0, P_R > 0, \\ & \beta_i + \sum_{j=i+1}^{N-1} \beta_j = 1 \text{ and } \beta_i > \sum_{j=i+1}^{N-1} \beta_j, \\ & 1 > \beta_i > \beta_N > 0 \text{ and } 0 < d_i, d_N. \end{aligned} \tag{46}$$

By setting $\Omega_{h_i} = \frac{1}{d_i^v}$ and $\Omega_g = \frac{1}{(1-d_i)^v}$, and substituting into (37), the following expression is obtained

$$\begin{aligned} \mathsf{P}_{\text{out}}^{\text{up,i,HD}}\left(\gamma_{\text{th,i}}^{\text{HD}}\right) = d_i^v \Bigg(& \frac{(1-N)\gamma_{\text{th,i}}^{\text{HD}} \mathrm{P_s} \Omega_{\mathrm{h_j}} \sum_{\mathrm{j=i+1}}^{\mathrm{N-1}} \beta_{\mathrm{j}}}{P_S \beta_i} \\ & + \frac{K P_F \Omega_{f_k} \sum_{k=1}^{K} \alpha_k \gamma_{\text{th,i}}^{\text{HD}}}{P_S \beta_i} \\ & + \frac{(1-i) P_s \Omega_{h_\ell} \sum_{\ell=1}^{i-1} \beta_\ell \gamma_{\text{th,i}}^{\text{HD}}}{P_S \beta_i} \\ & + \frac{1}{P_S \beta_i} \Bigg) + (1-d_i)^v \\ & \times \left(\frac{S P_M \Omega_{m_s} \sum_{s=1}^{S} \theta_s \gamma_{\text{th,i}}^{\text{HD}}}{P_R \beta_i} + \frac{\gamma_{\text{th,i}}^{\text{HD}}}{P_R \beta_i} \right) \end{aligned} \tag{47}$$

Before proceeding, we define $A = \frac{(1-N)\gamma_{\text{th,i}}^{\text{HD}} \mathrm{P_s} \Omega_{\mathrm{h_j}} \sum_{\mathrm{j=i+1}}^{\mathrm{N-1}} \beta_{\mathrm{j}}}{P_S \beta_i} + \frac{K P_F \Omega_{f_k} \sum_{k=1}^{K} \alpha_k \gamma_{\text{th,i}}^{\text{HD}}}{P_S \beta_i} + \frac{(1-i) P_s \Omega_{h_\ell} \sum_{\ell=1}^{i-1} \beta_\ell \gamma_{\text{th,i}}^{\text{HD}}}{P_S \beta_i} + \frac{1}{P_S \beta_i}$ and $B = \frac{S P_M \Omega_{m_s} \sum_{s=1}^{S} \theta_s \gamma_{\text{th,i}}^{\text{HD}}}{P_R \beta_i} + \frac{\gamma_{\text{th,i}}^{\text{HD}}}{P_R \beta_i}$. Then, by differentiating (37) with respect to d_i, the following expression is acquired

$$\frac{\partial \mathcal{L}\left(\mathsf{P}_{\text{out}}^{\text{up,i,HD}}\left(\gamma_{\text{th,i}}^{\text{HD}}\right)\right)}{\partial d_i} = v d_i^{v-1} A + v\,(1-d_i)^{v-1} B \tag{48}$$

Setting the obtained result to zero, the normalized location of U_i is obtained as $d_i = 1 \Big/ \left(\left(\frac{A}{B}\right)^{\frac{1}{v-1}} + 1 \right)$ and by definition, the normalized location of relay $\rightarrow$ BS is obtained as $1 - 1 \Big/ \left(\left(\frac{A}{B}\right)^{\frac{1}{v-1}} + 1 \right)$. Likewise, the normalized location of U_N is obtained as $d_N = 1 \Big/ \left(\left(\frac{C}{D}\right)^{\frac{1}{v-1}} + 1 \right)$ and by definition, the normalized location of relay $\rightarrow$ BS is obtained as $1 - 1 \Big/ \left(\left(\frac{C}{D}\right)^{\frac{1}{v-1}} + 1 \right)$, where $C = \frac{K P_F \Omega_{f_k} \sum_{k=1}^{K} \alpha_k \gamma_{\text{th,N}}^{\text{HD}}}{P_S \beta_N} + \frac{(1-N) P_s \Omega_{h_\ell} \sum_{\ell=1}^{N-1} \beta_\ell \gamma_{\text{th,N}}^{\text{HD}}}{P_S \beta_N} + \frac{\gamma_{\text{th,N}}^{\text{HD}}}{P_S \beta_N}$ and $D = \frac{S P_M \Omega_{m_s} \sum_{s=1}^{S} \theta_s \gamma_{\text{th,N}}^{\text{HD}}}{P_R \beta_N} + \frac{\gamma_{th,N}^{HD}}{P_R \beta_N}$.

Regarding FD, following a similar process to the HD mode, the normalized location of U_i is obtained as: $d_i = 1 \Big/ \left(\left(\frac{E}{F}\right)^{\frac{1}{v-1}} + 1 \right)$ and by definition, the normalized location of relay $\rightarrow$ BS is obtained as $1 - 1 \Big/ \left(\left(\frac{E}{F}\right)^{\frac{1}{v-1}} + 1 \right)$. where $E = \frac{(1-N)\mathrm{P_s} \Omega_{\mathrm{h_j}} \sum_{\mathrm{j=i+1}}^{\mathrm{N-1}} \beta_{\mathrm{j}} \gamma_{\text{th,i}}^{\text{FD}}}{P_S \beta_i} + \frac{K P_F \Omega_{f_k} \sum_{k=1}^{K} \alpha_k \gamma_{\text{th,i}}^{\text{FD}}}{P_S \beta_i} + \frac{P_R \Omega_c \gamma_{\text{th,i}}^{\text{FD}}}{P_S \beta_i} + \frac{(1-i) \mathrm{P_s} \Omega_{\mathrm{h}_\ell} \sum_{\ell=1}^{\mathrm{i-1}} \beta_\ell \gamma_{\text{th,i}}^{\text{FD}}}{P_S \beta_i} + \frac{\gamma_{\text{th,i}}^{\text{FD}}}{P_S \beta_i}$ and $F = \frac{S P_M \Omega_{m_s} \sum_{s=1}^{S} \theta_s \gamma_{\text{th,i}}^{\text{FD}}}{P_R \beta_i} + \frac{\gamma_{\text{th,i}}^{\text{FD}}}{P_R \beta_i}$. $d_N = 1 \Big/ \left(\left(\frac{G}{H}\right)^{\frac{1}{v-1}} + 1 \right)$ and by definition, the normalized location of relay $\rightarrow$ BS is obtained as $1 - 1 \Big/ \left(\left(\frac{G}{H}\right)^{\frac{1}{v-1}} + 1 \right)$. where $G = \frac{K P_F \Omega_{f_k} \sum_{k=1}^{K} \alpha_k \gamma_{\text{th,N}}^{\text{FD}}}{P_S \beta_N} + \frac{P_R \Omega_c \gamma_{\text{th,N}}^{\text{FD}}}{P_S \beta_N} + \frac{(1-N) P_s \Omega_{h_\ell} \sum_{\ell=1}^{N-1} \beta_\ell \gamma_{\text{th,N}}^{\text{FD}}}{P_S \beta_N} + \frac{\gamma_{\text{th,N}}^{\text{FD}}}{P_S \beta_N}$ and $H = \frac{S P_M \Omega_{m_s} \sum_{s=1}^{S} \theta_s \gamma_{\text{th,N}}^{\text{FD}}}{P_R \beta_N} + \frac{\gamma_{\text{th,N}}^{\text{FD}}}{P_R \beta_N}$.

B. OPTIMIZED POWER ALLOCATION UNDER FIXED RELAY LOCATION

Here, the optimal transmit power and power allocation coefficients, minimizing the system level outage performance, are derived. In this regard, the optimization problem is formulated as

$$\begin{aligned} \underset{P_S, P_R, \beta_i}{\text{minimize}} \quad & \mathsf{P}_{\text{out}}^{\text{up,i,HD}}\left(\gamma_{\text{th,i}}^{\text{HD}}\right) \\ \text{subject to} \quad & N \times P_S + P_R = P_T \text{ and } P_S > 0, P_R > 0, \\ & \beta_i + \sum_{j=i+1}^{N-1} \beta_j = 1 \text{ and } \beta_i > \sum_{j=i+1}^{N-1} \beta_j, \\ & 1 > \beta_i > \beta_N > 0. \end{aligned} \tag{49}$$

By performing a variable change, i.e. $P_R = P_T - N \times \mathrm{P_S}$, and substituting into the derived asymptotic CDF expression of $\bar{\mathsf{P}}_{\text{out}}^{\text{up,i-th,HD}}(\gamma_{\text{th,i}}^{\text{HD}})$, the following expression is obtained

$$\mathsf{P}_{\text{out}}^{\text{up,i,HD}}\left(\gamma_{\text{th,i}}^{\text{HD}}\right) = \left(1 - \left(P_S^{-1} E_2 + E_3 \left(P_T - N \times \mathrm{P_S}\right)^{-1}\right)\right) \tag{50}$$

where $E_2 = \frac{\gamma_{th,i}^{HD}}{\Omega_{h_i}\beta_i}$ and $E_3 = \frac{\gamma_{th,i}^{HD}}{\Omega_g\beta_i}$. Next, by differentiating with respect to P_S, the following expression is acquired

$$\frac{\partial \mathcal{L}\left(\mathsf{P}_{\text{out}}^{\text{up,i,HD}}\left(\gamma_{\text{th,i}}^{\text{HD}}\right)\right)}{\partial P_S} = \left(1-\left(E_2 P_S^{-2} + E_3\left(P_T - N\times \text{P}_\text{S}\right)^{-2} N\right)\right) \tag{51}$$

Setting the obtained result to zero, the optimized transmit powers are obtained as $P_S^* = \frac{P_T}{\sqrt{\frac{E_2}{E_3 N}+N}}$, and $P_R^* = P_T - \frac{N\times P_T}{\sqrt{\frac{E_2}{E_3 N}+N}}$. In a similar way, the N-th user's optimum transmit powers can also be obtained by changing the variables in E_2 and E_3 terms. Regarding the FD counterpart, the optimized transmit powers are obtained as: $P_S^* = \frac{P_T}{\sqrt{\frac{E_4}{E_5 N}+N}}$, and $P_R^* = P_T - \frac{N\times P_T}{\sqrt{\frac{E_4}{E_5 N}+N}}$, where $E_4 = \frac{\gamma_{th,i}^{FD}}{\Omega_{h_i}\beta_i}$ and $E_5 = \frac{\gamma_{th,i}^{FD}}{\Omega_g\beta_i}$. Likewise, the N-th user's optimum transmit powers can also be obtained by changing the variables in E_4 and E_5 terms. Regarding the power allocation coefficients optimization, first, $P_S = \left(\beta_i + \sum_{j=i+1}^{N-1}\beta_j\right)\frac{P_T}{N}$ and $P_R = \left(1-\beta_i - \sum_{j=i+1}^{N-1}\beta_j\right)\frac{P_T}{N}$ are defined. Then, substituting these expressions into the last term of the asymptotic CDF expression in (37), the following expression is obtained

$$\mathsf{P}_{\text{out}}^{\text{up,i,HD}}\left(\gamma_{\text{th,i}}^{\text{HD}}\right) = E_6\left(\left(\beta_i + \sum_{j=i+1}^{N-1}\beta_j\right)\frac{P_T}{N}\beta_i\right)^{-1} + E_7\left(\left(1-\beta_i - \sum_{j=i+1}^{N-1}\beta_j\right)\frac{P_T}{N}\beta_i\right)^{-1}, \tag{52}$$

where $E_6 = \frac{\gamma_{th,i}^{HD}}{\Omega_{h_i}}$ and $E_7 = \frac{\gamma_{th,i}^{HD}}{\Omega_g}$. Then, differentiating (52) with respect to β_i and setting the obtained result to zero, the expression below is acquired

$$\begin{aligned}\frac{\partial \mathcal{L}\left(\mathsf{P}_{\text{out}}^{\text{up,i,HD}}(\gamma_{\text{th,i}}^{\text{HD}})\right)}{\partial \beta_i} = &- E_6\left(\left(\beta_i + \sum_{j=i+1}^{N-1}\beta_j\right)\frac{P_T}{N}\beta_i\right)^{-2} \\ &\times\left(2\beta_i\frac{P_T}{N} + \sum_{j=i+1}^{N-1}\beta_j\frac{P_T}{N}\right) \\ &- E_7\left(\left(1-\beta_i - \sum_{j=i+1}^{N-1}\beta_j\right)\frac{P_T}{N}\beta_i\right)^{-2} \\ &\times\left(\frac{P_T}{N} - 2\beta_i\frac{P_T}{N} - \sum_{j=i+1}^{N-1}\beta_j\frac{P_T}{N}\right)\end{aligned} \tag{53}$$

Utilizing $\left(2\beta_i\frac{P_T}{N} + \sum_{j=i+1}^{N-1}\beta_j\frac{P_T}{N}\right)$ and setting it to zero, β_i and $\sum_{j=i+1}^{N-1}\beta_j$ are obtained as $1/3$ and $2/3$, respectively. However, the obtained result is not consistent with the constraint. Therefore, differentiating with respect to $\sum_{j=i+1}^{N-1}\beta_j$ and setting the obtained result to zero, β_i and $\sum_{j=i+1}^{N-1}\beta_j$ are obtained as $2/3$ and $1/3$, respectively. Note that by expanding $\sum_{j=i+1}^{N-1}\beta_j$ term based on the number of the user terminals in the system model and differentiating (52) with respect to each user's power allocation coefficients and setting the obtained result to zero and also taking into consideration the constraints, which are presented in (49), the other users' power allocation coefficients can be obtained.

VII. NUMERICAL RESULTS

In this section, we evaluate the impact of various parameters on the network performance and verify the analytical and asymptotic expressions through Monte-Carlo simulations using Matlab©. Two- and three-user uplink relay-aided network cases are considered and each time, 10^6 channel realizations are generated. Also, two scenarios are considered involving optimized and non-optimized parameters. In the first scenario, power allocation coefficients are non-optimized and their values are set as $\beta_i = 9/10$ and $\sum_{j=i+1}^{N-1}\beta_j = 1/10$. Then, in the second scenario, based on optimized power allocation coefficients, we set β_i and $\sum_{j=i+1}^{N-1}\beta_j$ as $2/3$ and $1/3$, respectively, as presented in Section VI-B. The target rate $R_{th,i}$ is equal to 0.2 bps/Hz and 0.001 bps/Hz for near and far users, respectively. This hetereogeneity in the QoS of the near and far users can be mapped to scenarios with varying service requirements, e.g. a low-bitrate mission-critical service that must be delivered with high reliability and machine-to-machine service with higher spectral efficiency demands. Furthermore, in the results, a channel bandwidth $B = 1$ Hz is considered, i.e. throughput coincides with the spectral efficiency of the transmission, as defined in Section III-D. The number of non-orthogonal CCI terminals affecting the relay, K, and the BS, S, are set to $K = 0, 1, 2$ and $S = 0, 1, 2$, respectively. As user/CCI terminals are randomly deployed, the Euclidean distance between the near user and the relay d_i is set to 1 while for the far user, d_N is set to 10. In reference to optimization section, the normalized distances for the near and far users in HD mode are set as $d_i = 1\Big/\left(\left(\frac{A}{B}\right)^{\frac{1}{v-1}}+1\right)$ and $d_N = 1\Big/\left(\left(\frac{C}{D}\right)^{\frac{1}{v-1}}+1\right)$, respectively. Regarding the FD mode, the normalized distances for the near and far users are set as $d_i = 1\Big/\left(\left(\frac{E}{F}\right)^{\frac{1}{v-1}}+1\right)$ and $d_N = 1\Big/\left(\left(\frac{G}{H}\right)^{\frac{1}{v-1}}+1\right)$, respectively. For the Euclidean distance for the near and far randomly deployed CCI terminals, affecting the relay, d_k and d_K, they are set to 1 and 10, respectively. The path-loss exponents v for the near and far users are set to 2, 3. Likewise, the Euclidean distance for the near and far randomly deployed CCI terminals, degrading the BS's reception, d_s and

TABLE 3. Simulation Parameters

Parameter	Symbol	Value (Optimized)	Value (Non-Optimized)
Power allocation coefficient for i-th user, $i=1$, $N=2$	β_i	2/3	9/10
Power allocation coefficient for j-th user, $j=2$, $N=2$	$\sum_{j=i+1}^{N-1}\beta_j$	1/3	1/10
Power allocation coefficient for i-th user, $N=3$	β_i	1/3	5/10
Power allocation coefficient for j-th user, $N=3$	β_j	1/3	3/10
Power allocation coefficient for N-th user, $N=3$	β_N	1/3	2/10
Target-rate for i-th user, $i=1$, $N=2$, (HD/FD)	$R_{th,i}$	0.2 bps/Hz	0.2 bps/Hz
Target-rate for N-th user, $N=2$, (HD/FD)	$R_{th,N}$	0.001 bps/Hz	0.001 bps/Hz
Target-rate for i-th user, $i=1$, $N=3$, (HD/FD)	$R_{th,i}$	0.2 bps/Hz	0.2 bps/Hz
Target-rate for j-th user, $j=2$, $N=3$, (HD/FD)	$R_{th,j}$	0.001 bps/Hz	0.001 bps/Hz
Target-rate for N-th user, $N=3$, (HD/FD)	$R_{th,N}$	0.0001 bps/Hz	0.0001 bps/Hz
Target threshold-rate for i-th user, $i=1$, $N=2$ (HD)	$\gamma_{th,i}^{HD}$	$2^{2R_{th,i}}-1$ bps/Hz	$2^{2R_{th,i}}-1$ bps/Hz
Target threshold-rate for N-th user, $N=2$ (HD)	$\gamma_{th,N}^{HD}$	$2^{2R_{th,N}}-1$ bps/Hz	$2^{2R_{th,N}}-1$ bps/Hz
Target threshold-rate for i-th user, $N=3$, (HD)	$\gamma_{th,i}^{HD}$	$2^{2R_{th,i}}-1$ bps/Hz	$2^{2R_{th,i}}-1$ bps/Hz
Target threshold-rate for j-th user, $N=3$, (HD)	$\gamma_{th,j}^{HD}$	$2^{2R_{th,j}}-1$ bps/Hz	$2^{2R_{th,j}}-1$ bps/Hz
Target threshold-rate for N-th user, $N=3$, (HD)	$\gamma_{th,N}^{HD}$	$2^{2R_{th,N}}-1$ bps/Hz	$2^{2R_{th,N}}-1$ bps/Hz
Target threshold-rate for i-th user, $i=1$, $N=2$ (FD)	$\gamma_{th,i}^{FD}$	$2^{R_{th,i}}-1$ bps/Hz	$2^{R_{th,i}}-1$ bps/Hz
Target threshold-rate for N-th user, $N=2$ (FD)	$\gamma_{th,N}^{FD}$	$2^{R_{th,N}}-1$ bps/Hz	$2^{R_{th,N}}-1$ bps/Hz
Target threshold-rate for i-th user, $N=3$, (FD)	$\gamma_{th,i}^{FD}$	$2^{R_{th,i}}-1$ bps/Hz	$2^{R_{th,i}}-1$ bps/Hz
Target threshold-rate for j-th user, $N=3$, (FD)	$\gamma_{th,j}^{FD}$	$2^{R_{th,j}}-1$ bps/Hz	$2^{R_{th,j}}-1$ bps/Hz
Target threshold-rate for N-th user, $N=3$, (FD)	$\gamma_{th,N}^{FD}$	$2^{R_{th,N}}-1$ bps/Hz	$2^{R_{th,N}}-1$ bps/Hz
The level of residual self-interference (FD)	λ	0.2	0.2
The level of residual interference (HD/FD)	λ_ℓ	0.1	0.1
Channel bandwidth	B	1 Hz	1 Hz
Number of non-orthogonal CCI at relay	K	$0,1,2$	$0,1,2$
Number of non-orthogonal CCI at BS	S	$0,1,2$	$0,1,2$
Euclidean distance between the near user and the relay (HD)	d_i	$1/\left(\left(\frac{A}{B}\right)^{\frac{1}{v-1}}+1\right)$	1
Euclidean distance between the far user and the relay (HD)	d_N	$1/\left(\left(\frac{C}{D}\right)^{\frac{1}{v-1}}+1\right)$	10
Euclidean distance between the near user and the relay (FD)	d_i	$1/\left(\left(\frac{E}{F}\right)^{\frac{1}{v-1}}+1\right)$	1
Euclidean distance between the far user and the relay (FD)	d_N	$1/\left(\left(\frac{G}{H}\right)^{\frac{1}{v-1}}+1\right)$	10
Euclidean distance for the near CCI terminals $\rightarrow$ relay	d_k	1	1
Euclidean distance for the far CCI terminals $\rightarrow$ relay	d_K	10	10
Euclidean distance for the near CCI terminals $\rightarrow$ BS	d_s	1	1
Euclidean distance for the far CCI terminals $\rightarrow$ BS	d_S	10	10
The path-loss exponent for the near user	ν	2	2
The path-loss exponent for the near user	ν	3	3

d_S, they are set to 1 and 10, respectively. The path-loss exponents for the near and far users are set to 2, 3. k-th and s-th CCI terminals transmit powers, which are P_J and P_F, are set to $P_T d_k^{-v}$ and $P_T d_s^{-v}$, respectively. The residual self-interference is modelled as $\sigma_c^2 P_R.^{\lambda-1}$, where λ takes values between $0 \leq \lambda \leq 1$ [56, Eq. (8)] depending the residual self-interference mitigation level. Here, λ is set to 0.2 in the performance analysis while the level of residual interference, λ_ℓ, is set to 0.1. For convenience, Table 3 provides all the simulation parameters, together with their descriptions and values for the two- and three-user scenarios that we investigate.

A. OUTAGE PROBABILITY

Fig. 2 presents the optimized and non-optimized outage probability performance of the near user along with HD and FD modes under i.i.d CCI, $K=S=M=\{0,1,2\}$, $v=\{2,3\}$, and $R_{th,1}=0.2$ bps/Hz. Results reveal that in the low SNR regime, the CCI along with the different path-loss exponents and $d=10$ do not have any significant effect on the outage performance of optimized and non-optimized U_1. Throughout the SNR range, the non-optimized case achieves a slightly better outage performance, as a higher power allocation value is employed. Moreover, the HD mode achieves slightly better outage performance compared to its counterpart, the FD

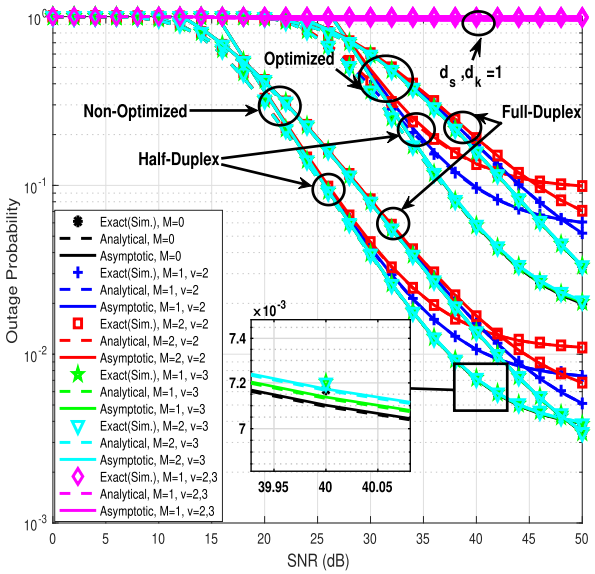

FIGURE 2. Optimized and non-optimized outage probability performance of the near user along with HD and FD modes under i.i.d CCI, $K = S = M = \{0, 1, 2\}$, $d = \{1, 10\}$, $v = \{2, 3\}$, and $R_{th,1} = 0.2$ bps/Hz.

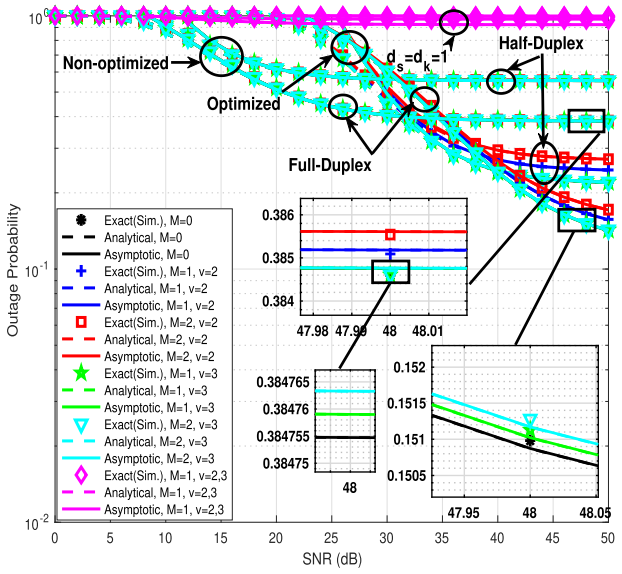

FIGURE 3. Optimized and non-optimized outage probability performance of the far user along with HD and FD modes under i.i.d CCI, $K = S = M = \{0, 1, 2\}$, $d = \{1, 10\}$, $v = \{2, 3\}$, and $R_{th,2} = 0.001$ bps/Hz.

mode, in low and mid SNR regimes. However, in high SNR regimes, the FD mode offers improved outage performance in comparison to the HD mode. The performance differences occur because of the pre-log factor differences between the two modes and the residual self-interference effects.

Still, for high SNR regime, an outage floor is observed for all cases. In addition, in $K = S = M = 0$ case, the outage floor is observed because of the other users' interference within the system model. U_1 does not experience any imperfect SIC effects because of the order of the decoding process. Additionally, regardless of the number of CCI terminals, the path-loss exponent determines the CCI severity, as the outage floor is observed much earlier when $v = 2$.

Fig. 3 presents the optimized and non-optimized outage probability performance of the far user U_2 along with HD and FD modes, under i.i.d CCI, $K = S = M = \{0, 1, 2\}$, $d = \{1, 10\}$, $v = \{2, 3\}$, and $R_{th,2} = 0.001$ bps/Hz. It can be observed that in low and mid SNR regime, the non-optimized case achieves slightly better outage performance than its counterpart for high SNR. Nonetheless, due to the CCI's detrimental effects, the non-optimized curves sharply saturates in the high SNR regime. Moreover, for high SNR values, the optimized case achieves significantly better outage performance than the non-optimized one, as higher power is allocated to U_2's transmission. Moreover, the FD mode achieves slightly reduced outage probability than HD mode for both low and high SNR. This performance gain occurs because of the pre-log factor differences between the two duplexing modes and the residual self-interference. Regardless of the operating mode, the $K = S = M = 0$ case also experiences performance degradation as a result of imperfect SIC. As it was observed for U_1, the path-loss exponent is the dominant factor of the CCI severity. Moreover, when the CCI terminals' Euclidean distances towards the relay and the BS is set to 1, the far user is nearly in complete outage.

We further investigated the outage performance of relay-aided uplink NOMA with $N = 3$, considering various QoS requirement for user terminals. Results in Fig. 4 reveal that increasing the number of user terminals degrades the far-user's outage performance, as the amount of the interference at the BS to detect the far-user signal increases. As a result, adopting a user-pairing uplink strategy where the number of users is equal to two provides the best trade-off among outage performance and spectral efficiency.

Fig. 5 presents the optimized outage probability performance comparison of the far-user under perfect SIC and imperfect SIC in HD and FD modes. More specifically, Fig. 5 shows that ISIC causes system coding gain losses and causes saturation on the perfect SIC counterpart in high SNR regimes. This behaviour can be attributed to the residual interference caused by the imperfect SIC. Moreover, as clearly shown in Fig. 3, the FD mode achieves slightly reduced outage performance than HD mode. This observation occurs because of the pre-log factor differences between the two duplexing modes and the residual self-interference.

B. ERROR PROBABILITY

Fig. 6 depicts the optimized and non-optimized error probability performance of near user U_1 for both duplexing modes, under i.i.d CCI, $K = S = M = \{0, 1, 2\}$, $d = \{1, 10\}$, $v = \{2, 3\}$, and $R_{th,1} = 0.2$ bps/Hz. As it was observed in the outage curves, the optimized error probability is reduced compared to the non-optimized case for increasing SNR values.

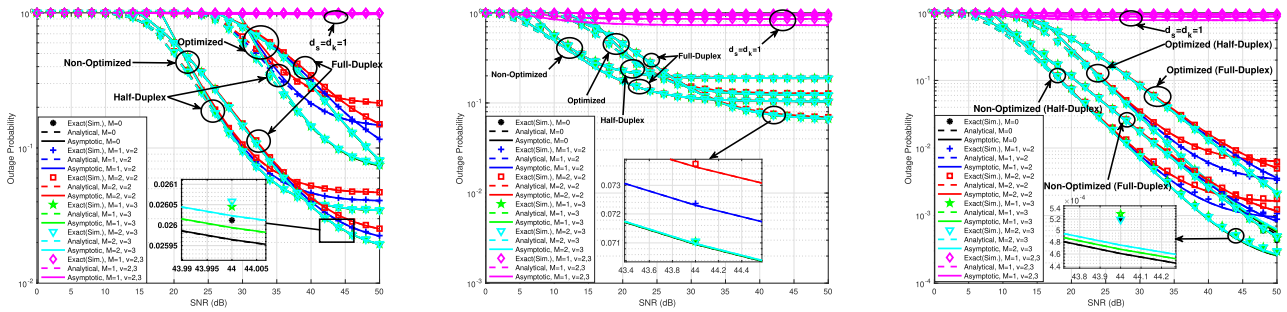

(a) (b) (c)

FIGURE 4. Outage probability performance comparison for HD and FD-based relay-aided NOMA system with $N = 3$, $R_{th,1} = 0.2$, $R_{th,2} = 0.001$, $R_{th,3} = 0.0001$ bps/Hz, and for optimized and non-optimized scenarios. (a) $R_{th,1} = 0.2$, (b) $R_{th,2} = 0.001$, (c) $R_{th,3} = 0.0001$ bps/Hz.

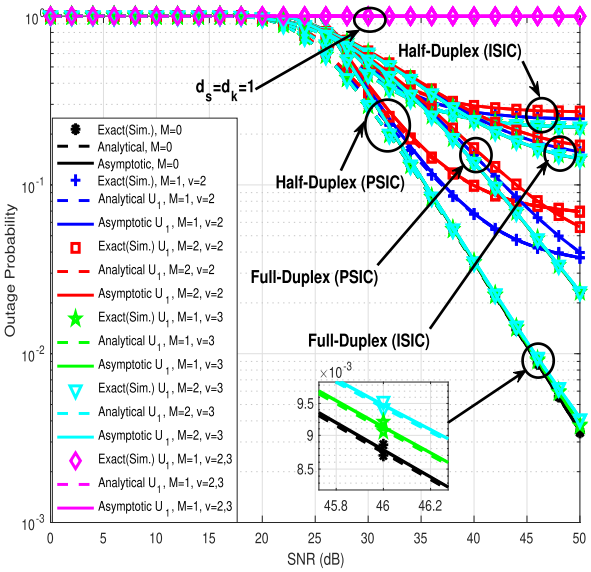

FIGURE 5. Optimized perfect and imperfect SIC outage probability performance of the far user along with HD and FD modes under i.i.d CCI, $K = S = M = \{0, 1, 2\}$, $d = \{1, 10\}$, $v = \{2, 3\}$, and $R_{th,2} = 0.001$ bps/Hz.

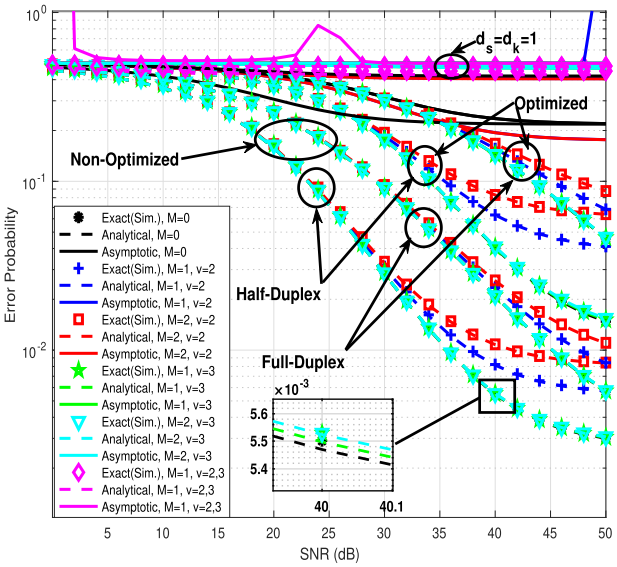

FIGURE 6. Optimized and non-optimized error probability performance of the near user along with HD and FD modes under i.i.d CCI, $K = S = M = \{0, 1, 2\}$, $d = \{1, 10\}$, $v = 2$, and $R_{th,1} = 0.2$ bps/Hz.

This is observed as a consequence of the power allocation between the two cases. Fig. 6 also shows that HD operation achieves a slightly better error probability performance than the FD mode. This observation occurs because of the pre-log factor differences between the two duplexing modes and residual self-interference effects in FD mode. All performance curves including $K = S = M = \{0\}$, tend to saturate for high SNR because of the decoding order. Finally, when the Euclidean distance for CCI terminals, which are $d_s = d_k$, is set to 1, the error probability performance curves sharply saturates for all SNR values.

Fig. 7 shows the optimized and non-optimized error probability performance of the far user U_2 for with HD mode, under i.i.d CCI, $K = S = M = \{0, 1, 2\}$, $d = \{1, 10\}$, $v = \{2, 3\}$, and $R_{th,2} = 0.001$ bps/Hz. It is revealed that the error probability saturates for very high SNR values. This behavior stems from the impact of imperfect SIC and non-orthogonal CCI on the uplink NOMA-based relay network. In addition, when the Euclidean distance for CCI terminals is set to 1, the performance curves saturate along the SNR and causes system coding gain losses. Results also show that the optimized error probability performance is slightly better over the non-optimized cases due to power allocation coefficient differences.

Fig. 8 includes the optimized and non-optimized FD relay-assisted error probability performance of the far user U_2 for the FD mode, under i.i.d CCI, $K = S = M = \{0, 1, 2\}$, $d = \{1, 10\}$, $v = \{2, 3\}$, and $R_{th,2} = 0.001$ bps/Hz. Results indicate that the error probability performance saturates for very high error SNR values. This observation occurs because of the severe non-orthogonal CCI and imperfect SIC impact on the system performance. From the comparisons in Figs. 6 and 7 it can be observed that HD and FD modes provide almost identical error probabilities.

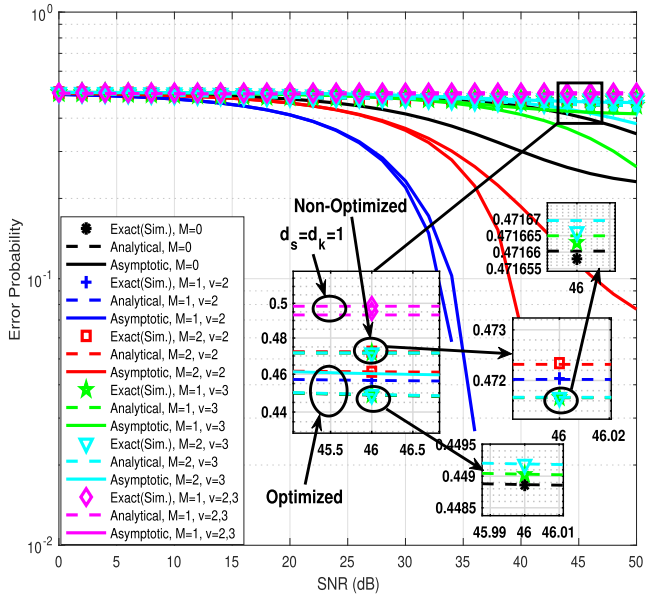

FIGURE 7. Optimized and non-optimized error probability performance of the far user along with HD mode under i.i.d CCI, $K = S = M = \{0, 1, 2\}$, $d = \{1, 10\}$, $v = 2$, and $R_{th,2} = 0.001$ bps/Hz.

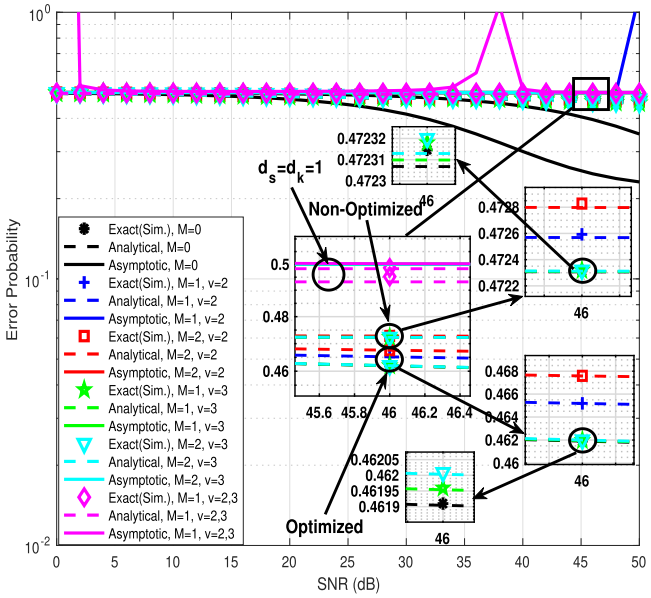

FIGURE 8. Optimized and non-optimized error probability performance of the far user along with FD mode under i.i.d CCI, $K = S = M = \{0, 1, 2\}$, $d = \{1, 10\}$, $v = 2$, and $R_{th,2} = 0.001$ bps/Hz.

C. THROUGHPUT

Here, the throughput performance is evaluated for the near and far users for both HD and FD modes. Fig. 9 depicts the throughput performance of the optimized and non-optimized cases for the near user, assuming i.i.d CCI, $K = S = M = \{0, 1, 2\}$, $d = \{1, 10\}$, $v = \{2, 3\}$, and $R_{th,1} = 0.2$ bps/Hz. In the low SNR regime, the non-optimized U_1 achieves slightly higher throughput than the optimized counterpart, as a higher power allocation coefficient value is adopted. Results also

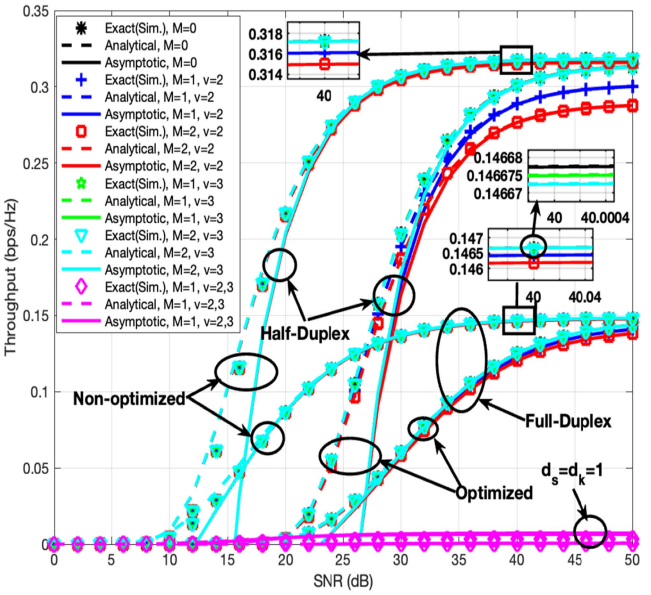

FIGURE 9. Optimized and non-optimized throughput performance of the near user along with HD and FD modes under i.i.d CCI, $K = S = M = \{0, 1, 2\}$, $d = \{1, 10\}$, $v = \{2, 3\}$, and $R_{th,1} = 0.2$ bps/Hz.

show that the relay-assisted network experiences improved throughput performance when the relay terminal operates in HD mode instead of FD. Nonetheless, an increased number of CCI terminals along with $d = 10$ and $v = 2, 3$ cause small coding gain losses compared to the case without CCI, i.e. $K = S = M = 0$. Then, when d is set to 1, regardless of the number of CCI terminals and the values of path-loss exponent, very low throughput is achieved. In this case, the non-optimized case with a larger power allocation coefficient benefits U_1's throughput.

Next, Fig. 10 illustrates the optimized and non-optimized throughput performance of the far user for the two duplexing modes under i.i.d CCI, $K = S = M = \{0, 1, 2\}$, $d = \{1, 10\}$, $v = \{2, 3\}$, and $R_{th,2} = 0.001$ bps/Hz. As expected, the throughput of U_2 under optimized parameters is higher than the non-optimized case, as larger power is allocated and the relay's position is optimized, for both HD and FD modes. In addition, independently of the number of CCI terminals affecting the relay and the BS, when $d = 10$, all cases reach the throughput upper-bound at high SNR. Still, when $v = 3$, higher throughput is provided throughout the SNR range, as the CCI effect is reduced. When the CCI terminals are located closer to the receiver, i.e. $d = 1$, almost zero throughput is obtained, due to the very high CCI severity.

D. ENERGY EFFICIENCY

The energy efficiency performance of each user is examined under the impact of different network parameters. First, in Fig. 11, the optimized and non-optimized energy efficiency performance of the near user along with HD and FD modes are presented considering i.i.d CCI, $K = S = M = \{0, 1, 2\}$, $d = \{1, 10\}$, $v = \{2, 3\}$, $R_{th,1} = 0.2$ bps/Hz, and $P_S = P_R =$

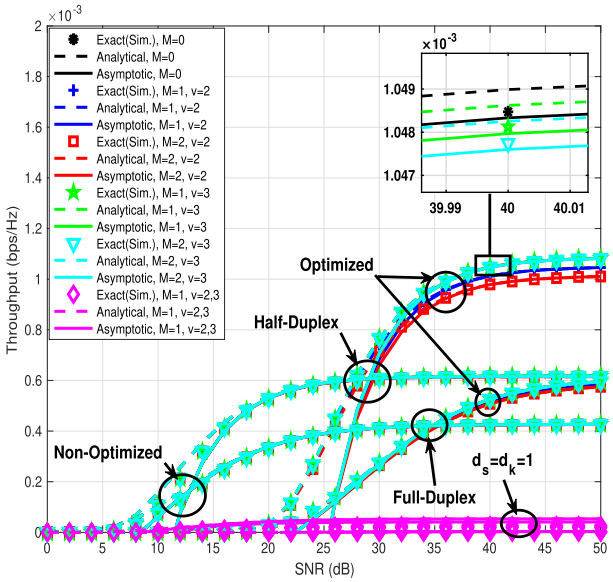

FIGURE 10. Optimized and non-optimized throughput performance of the far user along with HD and FD modes under i.i.d CCI, $K = S = M = \{0, 1, 2\}$, $d = \{1, 10\}$, $v = \{2, 3\}$, and $R_{th,2} = 0.001$ bps/Hz.

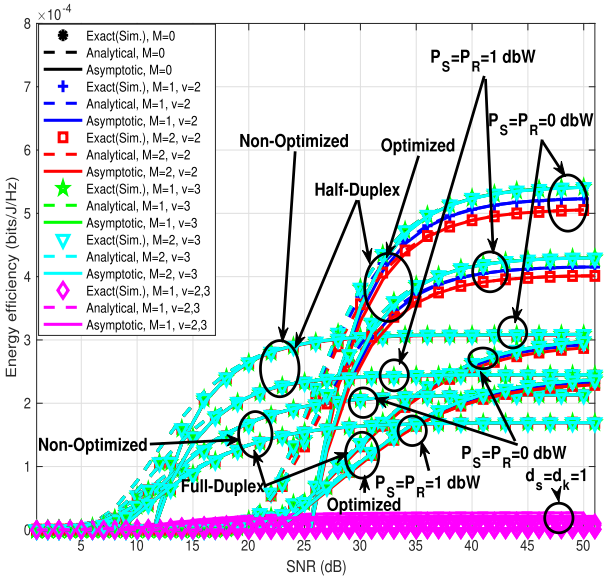

FIGURE 12. Optimized and non-optimized energy efficiency analysis of the far user along with HD and FD modes under i.i.d CCI, $K = S = M = \{0, 1, 2\}$, $d = \{1, 10\}$, $v = \{2, 3\}$, and $R_{th,2} = 0.001$ bps/Hz, and $P_S = P_R = \{0, 1\}$ dBW.

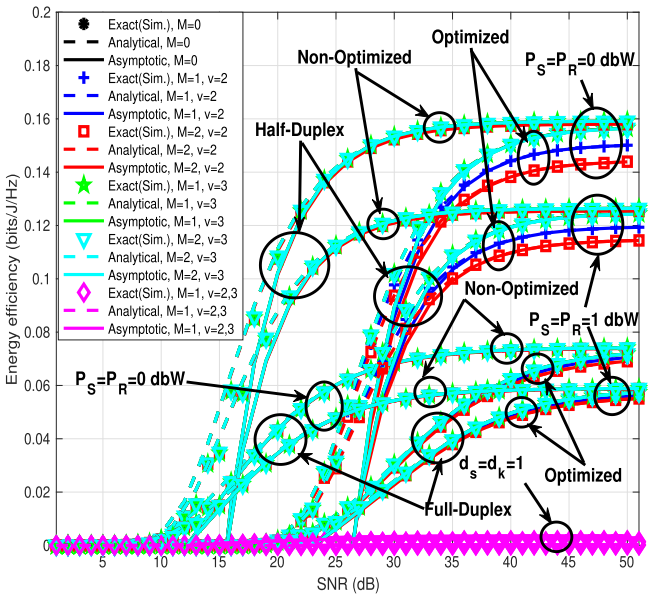

FIGURE 11. Optimized and non-optimized energy efficiency analysis of near user along with HD and FD modes under i.i.d CCI, $K = S = M = \{0, 1, 2\}$, $d = \{1, 10\}$, $v = \{2, 3\}$, $R_{th,1} = 0.2$ bps/Hz, and $P_S = P_R = \{0, 1\}$ dBW.

$\{0, 1\}$ dBW. It can be seen that similar behavior is observed regarding the impact of the number of CCI terminals and path-loss exponent value. Moreover, the HD mode achieves a slightly better performance than FD mode. Also, the non-optimized case demonstrates improved energy efficiency, as higher throughput is achieved due to the higher power allocation coefficient value. It must be noted that when the transmit power increases, lower energy efficiency is obtained, as a fixed rate transmission is considered and when SNR conditions improve, the target rate is achieved without additional power. Still, the optimized parameters are used and $P_S = P_R = 1$ dBW provides improved energy efficiency at low SNR over the case with non-optimized parameters and $P_S = P_R = 0$ dBW, as outages are avoided.

Fig. 12 presents the optimized and non-optimized energy efficiency analysis of the far user for both duplexing modes under i.i.d CCI, $K = S = M = \{0, 1, 2\}$, $d = \{1, 10\}$, $v = \{2, 3\}$, $R_{th,2} = 0.001$ bps/Hz, and $P_S = P_R = \{0, 1\}$ dBW. Here, the optimization of the network parameters results in improved energy efficiency for both HD and FD modes for the far user. In addition, results show that the NOMA relay network, operating in HD outperforms its FD counterpart. Also, due to the impact of imperfect SIC and CCI, the energy efficiency performance saturates for high SNR values. Furthermore, a higher path-loss exponent enables U_2 to achieve higher throughput, thus benefiting the energy efficiency of the transmission. Similar to the transmission of U_1 when higher transmit power is employed, energy efficiency decreases, since a fixed rate transmission is performed. Still, it can be seen that when optimized parameters are used and $P_S = P_R = 1$ dBW, the energy efficiency for low SNR surpasses the non-optimized case and $P_S = P_R = 0$ dBW, as the latter exhibits increased outages.

E. THE IMPACT OF USER LOCATION

Fig. 13 plots the optimized and non-optimized outage probability versus the normalized distance of the near user along with HD and FD modes, considering i.i.d CCI, $K = S = M = \{0, 1, 2\}$, $d = \{1, 10\}$, $v = 2, 3$, and $R_{th,1} = 0.2$ bps/Hz. Here, the non-optimized case offers slightly reduced outages over the optimized case for the same normalized distance value due

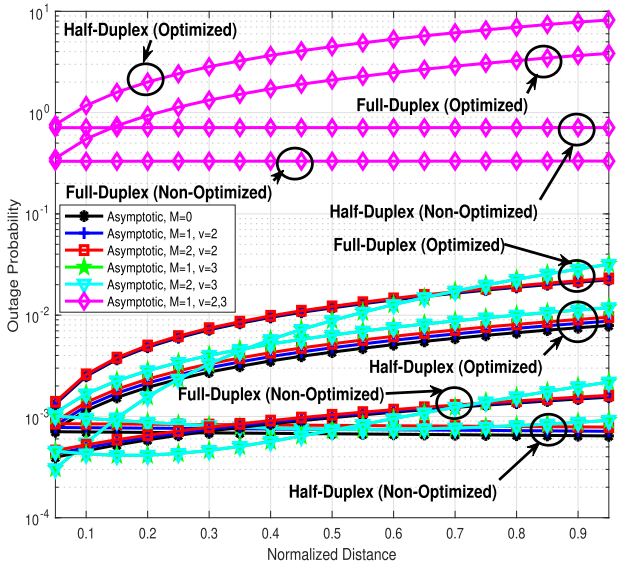

FIGURE 13. Optimized and non-optimized outage probability versus normalized distance performance of the near user along with HD and FD modes under i.i.d CCI, $K = S = M = \{0, 1, 2\}$, $d = \{1, 10\}$, $v = 2$, and $R_{th,1} = 0.2$ bps/Hz. SNR is set to 30 dB.

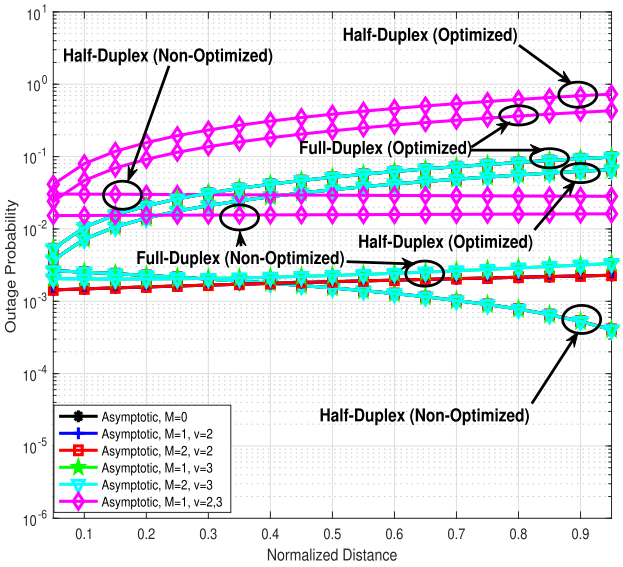

FIGURE 14. Optimized and non-optimized outage probability versus normalized distance performance of the far user along with HD and FD modes under i.i.d CCI, $K = S = M = \{0, 1, 2\}$, $d = \{1, 10\}$, $v = 2$, and $R_{th,2} = 0.001$ bps/Hz. SNR is set to 10 dB.

to the higher power allocation coefficient for both duplexing modes. It can be also seen that the outage performance of both cases improves when the normalized distance is equal to 1. Moreover, the HD mode provides reduced outage probability compared to the FD case.

Finally, Fig. 14 demonstrates the optimized and non-optimized outage probability versus the normalized distance of the far user for both HD and FD modes under i.i.d CCI, $K = 0, 1, 2$, $S = 0, 1, 2$, $d = 1, 10$, $v = 2, 3$, and $R_{th,2} = 0.001$ bps/Hz. Results demonstrate that the optimized case offers better outage performance over the non-optimized case for varying normalized distance values. This performance gap occurs due to the different power allocation coefficient values. In this comparison, it can be observed that the outage performance of optimized and non-optimized cases improves when the normalized distance reaches 0.5. However, the outage performance deteriorates when the distance is equal to 1.

VIII. CONCLUSION & FUTURE DIRECTIONS

Non-orthogonal multiple access (NOMA) is an important building block of forthcoming 6G networks comprising co-existing users and Internet-of-Things devices. As a result, increased levels of NOMA-related co-channel interference will arise. This paper has investigated the detrimental effects of randomly deployed CCI terminals communicating through NOMA on the performance of a half-duplex/full-duplex amplify-and-forward relay-assisted uplink network. More specifically, in our study, non-orthogonal CCI affected the reception of the relay and the base station. Performance was analyzed in terms of outage, error, throughput, energy efficiency, and asymptotic behaviour. Furthermore, in such a challenging setting, the Lagrangian multiplier optimization technique was employed to optimize the relay's location, the transmit power, and the power allocation coefficients for NOMA. The derived analytical and asymptotic expressions were evaluated and verified by means of Monte-Carlo-based computer simulations. The results revealed that the non-orthogonal CCI degrades the system performance severely and causes system coding gain losses in high SNR regimes.

This study can be further extended to several directions. First, hybrid schemes combining NOMA with sparse code multiple access can increase the sum-rate performance under the impact of non-orthogonal CCI [57]. Another important direction involves the study of cases where non-orthogonal CCI is not detrimental, and strategies for interference exploitation can be devised. Finally, considering full-duplex relay operation, power control, and power allocation for NOMA can be optimized by adopting reinforcement learning towards avoiding channel state information acquisition and reducing coordination overheads [58], [59].

APPENDIX
PROOF OF PROPOSITION 1

By leveraging (9) and applying probability properties, we derive the following expressions:

$$F^{\text{up}}_{\gamma_{\text{x}_\text{i}}}\left(\gamma^{\text{HD}}_{\text{th,i}}\right) = \Pr\left(\beta_i \min\left(\text{A}_1, \text{B}_1\right) \leq \underbrace{\gamma^{HD}_{\text{th,i}}}_{2^{2\text{R}x_\text{i}}-1}\right)$$

$$= \Pr\left(\beta_i \min\left(\frac{\gamma_{\text{x}_\text{i}}}{\left(\sum_{\text{j}=\text{i}+1}^{\text{N}-1} \beta_\text{j}\gamma_{\text{x}_\text{J}} + \delta\right)}\right.\right.,$$

$$\left.\left.\left.\frac{\gamma_y}{\left(\sum_{s=1}^{S}\theta_s\gamma_M+1\right)}\right)\le\gamma_{\mathrm{th,i}}^{HD}\right)\right.$$

$$=1-\mathrm{P_R}\left(\gamma_{\mathrm{x_i}}\ge\frac{\gamma_{\mathrm{th,i}}^{\mathrm{HD}}}{\beta_{\mathrm{i}}}\left(\sum_{\mathrm{j=i+1}}^{\mathrm{N-1}}\beta_{\mathrm{j}}\gamma_{\mathrm{x_J}}+\delta\right),\right.$$

$$\left.\gamma_y\ge\frac{\gamma_{\mathrm{th,i}}^{HD}}{\beta_i}\left(\sum_{s=1}^{S}\theta_s\gamma_M+1\right)\right)$$

$$=1-\left(\left(1-F_{\gamma_{x_i}}\left(\frac{\gamma_{\mathrm{th,i}}^{HD}}{\beta_i}\left(\sum_{j=i+1}^{N-1}\beta_j\gamma_{x_J}+\delta\right)\right)\right)\right.$$

$$\left.\times\left(1-F_{\gamma_y}\left(\frac{\gamma_{\mathrm{th,i}}^{HD}}{\beta_i}\left(\sum_{s=1}^{S}\theta_s\gamma_M+1\right)\right)\right)\right) \tag{54}$$

Substituting the related CDF expressions, $F_{\gamma_{x_i}}(\gamma)=1-e^{-\frac{\gamma}{P_S\Omega_{h_i}}}$ and $F_{\gamma_y}(\gamma)=1-e^{-\frac{\gamma}{P_R\Omega_g}}$ [60], into (54), the following expressions are obtained.

$$=1-\mathbb{E}_{\gamma_{x_J},\gamma_{x_F},\gamma_{x_L},\gamma_{x_M}}\left[e^{-\gamma_{\mathrm{th,i}}^{HD}\left(\frac{\sum_{j=i+1}^{N-1}\beta_j\gamma_{x_J}+\delta}{P_S\Omega_{h_i}\beta_i}\right)}\right.$$

$$\left.\times\,e^{-\gamma_{\mathrm{th,i}}^{HD}\left(\frac{\sum_{s=1}^{S}\theta_s\gamma_M+1}{P_R\Omega_g\beta_i}\right)}\right|_{\gamma_{x_J},\gamma_{x_F},\gamma_{x_L},\gamma_{x_M}}\Bigg]$$

$$=1-e^{-\gamma_{\mathrm{th,i}}^{HD}\left(\frac{1}{P_S\Omega_{h_i}\beta_i}+\frac{1}{P_R\Omega_g\beta_i}\right)}$$

$$\times\int_0^\infty e^{-\gamma_{x_J}\left(\frac{\sum_{j=i+1}^{N-1}\beta_j\gamma_{\mathrm{th,i}}^{HD}}{P_S\Omega_{h_i}\beta_i}\right)}f_{\gamma_{x_J}}(\gamma_{x_J})\,d\gamma_{x_J}$$

$$\times\int_0^\infty e^{-\gamma_F\left(\frac{\sum_{k=1}^{K}\alpha_k\gamma_{\mathrm{th,i}}^{HD}}{P_S\Omega_{h_i}\beta_i}\right)}f_{\gamma_F}(\gamma_F)\,d\gamma_F$$

$$\times\int_0^\infty e^{-\gamma_{x_L}\left(\frac{\sum_{\ell=1}^{i-1}\beta_\ell\gamma_{\mathrm{th,i}}^{HD}}{P_S\Omega_{h_i}\beta_i}\right)}f_{\gamma_{x_L}}(\gamma_{x_L})\,d\gamma_{x_L}.$$

$$\times\int_0^\infty e^{-\gamma_{x_M}\left(\frac{\sum_{s=1}^{S}\theta_s\gamma_{\mathrm{th,i}}^{HD}}{P_R\Omega_g\beta_i}\right)}f_{\gamma_{x_M}}(\gamma_{x_M})\,d\gamma_{x_M}. \tag{55}$$

where $f_{\gamma_{x_J}}(\gamma_J)=\frac{\gamma_J^{N-2}}{(\mathrm{P}_s\Omega_{h_j})^{N-1}(N-2)!}e^{-\frac{\gamma_J}{\mathrm{P}_s\Omega_{h_j}}}$, $f_{\gamma_{x_L}}(\gamma_{x_L})=\frac{\gamma_{x_L}^{i-2}}{(\mathrm{P}_s\Omega_{h_\ell})^{i-1}(i-2)!}e^{-\frac{\gamma_{x_L}}{\mathrm{P}_s\Omega_{h_\ell}}}$, $f_{\gamma_F}(\gamma_F)=\frac{\gamma_F^{K-1}}{(\mathrm{P}_F\Omega_{f_k})^K(K-1)!}e^{-\frac{\gamma_F}{\mathrm{P}_F\Omega_{f_k}}}$ and $f_{\gamma_M}(\gamma_M)=\frac{\gamma_M^{S-1}}{(\mathrm{P}_M\Omega_{M_s})^S(S-1)!}e^{-\frac{\gamma_M}{\mathrm{P}_M\Omega_{m_s}}}$.

Regarding the CCI PDF, note that the sum of M i.i.d. Rayleigh distributions is Gamma distributed [60]. So, the Gamma distribution's PDF expression for γ_J and γ_F can be written as $f_{\gamma_J}(\gamma_J)=\frac{\gamma_J^{K-1}}{(\mathrm{P}_J\Omega_{f_k})^K(K-1)!}e^{-\frac{\gamma_J}{\mathrm{P}_J\Omega_{f_k}}}$, $f_{\gamma_F}(\gamma_F)=\frac{\gamma_F^{S-1}}{(\mathrm{P}_F\Omega_{m_s})^S(S-1)!}e^{-\frac{\gamma_F}{\mathrm{P}_F\Omega_{m_s}}}$ [60]. Substituting these expressions into (55) and solving the integral expressions with the help of [54, Eq. (3.310[11], 3.351.3)] lead to (21). In a similar way, utilizing (18) and considering a similar procedure, the N-th user's analytical derivations are obtained as in (22). Following a similar procedure as in the HD mode and also utilizing (19) and (20), the FD mode's outage probability analytical derivations for the i-th and N-th users are obtained as in (23) and (24), respectively.

PROOF OF PROPOSITION 2

Substituting (21) into (25) and using distributive properties and partial fraction decomposition, we obtain

$$\bar{\mathrm{P}}_{\mathrm{e}}^{i,HD}=\frac{1}{2\sqrt{\pi}}\int_0^\infty x^{-\frac{1}{2}}e^{-x}dx$$

$$-\frac{1}{2\sqrt{\pi}}\int_0^\infty x^{-\frac{1}{2}}e^{-x\left(\frac{1}{\mathrm{P_S}\Omega_{\mathrm{h_i}}\beta_{\mathrm{i}}}+\frac{1}{P_R\Omega_g\beta_i}+1\right)}$$

$$\times\left(1+x\frac{\Omega_{h_j}\sum_{j=i+1}^{N-1}\beta_j}{\Omega_{h_i}\beta_i}\right)^{1-N}$$

$$\times\left[\frac{\sum_{a=1}^{K}A_a}{\left(1+x\frac{\sum_{k=1}^{K}\alpha_kP_F\Omega_{f_k}}{\mathrm{P_S}\Omega_{\mathrm{h_i}}\beta_{\mathrm{i}}}\right)^a}+\frac{\sum_{b=1}^{i-1}B_b}{\left(1+x\frac{\sum_{\ell=1}^{i-1}\beta_\ell\Omega_{h_\ell}}{\Omega_{h_i}\beta_i}\right)^b}\right.$$

$$\left.+\frac{\sum_{c=1}^{S}C_c}{\left(1+x\frac{\sum_{s=1}^{S}\theta_sP_M\Omega_{m_s}}{P_R\Omega_g\beta_i}\right)^c}\right]dx. \tag{56}$$

where

$$A_a=y\to-\frac{\lim_{P_s\Omega_{h_i}\beta_i}}{\sum_{k=1}^{K}\alpha_kP_F\Omega_{f_k}}$$

$$\times\frac{\partial^{K-a}}{(K-a)!\partial y^{K-a}}\left(1+y\frac{\sum_{k=1}^{K}\alpha_kP_F\Omega_{f_k}}{P_s\Omega_{h_i}\beta_i}\right)^K\Phi,$$

$$B_b=y\to-\frac{\lim_{P_s\Omega_{h_i}\beta_i}}{\sum_{\ell=1}^{i-1}\beta_\ell P_s\Omega_{h_\ell}}\frac{\partial^{i-1-b}}{(i-1-b)\partial y^{i-1-b}}$$

$$\times\left(1+y\frac{\sum_{\ell=1}^{i-1}\beta_\ell P_s\Omega_{h_\ell}}{P_s\Omega_{h_i}\beta_i}\right)^{i-1}\Phi,$$

$$C_c = y \to -\frac{\lim_{P_R\Omega_g\beta_i}}{\sum_{s=1}^{S}\theta_s P_M \Omega_{m_s}} \frac{\partial^{S-c}}{(S-c)!\partial y^{S-c}} \times \left(1 + y\frac{\sum_{s=1}^{S}\theta_s P_M \Omega_{m_s}}{P_R\Omega_g\beta_i}\right)^{S} \Phi,$$

$$\Phi = \left[\frac{1}{\left(1 + y\frac{\sum_{k=1}^{K}\alpha_k P_F \Omega_{f_k}}{\mathrm{P}_s\Omega_{h_i}\beta_i}\right)^{K}\left(1 + y\frac{\sum_{\ell=1}^{1-i}\beta_\ell \mathrm{P}_s\Omega_{h_\ell}}{\mathrm{P}_s\Omega_{h_i}\beta_i}\right)^{i-1}} \times \frac{1}{\left(1 + y\frac{\sum_{s=1}^{S}\theta_s P_M \Omega_{m_s}}{P_R\Omega_g\beta_i}\right)^{S}}\right].$$

The first integral expression in (56) can be solved by means of [61, Eq. (3.326.2[10])] as $\Gamma(1/2) = \sqrt{\pi}$. By using the distributive properties and utilizing [62, Eq. (10, 11)], the following expressions can be obtained

$$\begin{aligned}
&\frac{\sum_{a=1}^{K} A_a}{\Gamma(N-1)\Gamma(a)} \\
&\times \int_0^{\infty} x^{-\frac{1}{2}} G_{0,1}^{1,0}\left(x\left(\frac{1}{\mathrm{P}_s\Omega_{h_i}\beta_i} + \frac{1}{P_R\Omega_g\beta_i} + 1\right) \middle| \begin{matrix} - \\ 0 \end{matrix}\right) \\
&\times G_{1,1}^{1,1}\left(x\frac{\mathrm{P}_s\Omega_{h_j}\sum_{j=i+1}^{N-1}\beta_j}{\mathrm{P}_s\Omega_{h_i}\beta_i} \middle| \begin{matrix} 2-N \\ 0 \end{matrix}\right) \\
&\times G_{1,1}^{1,1}\left(x\frac{\sum_{k=1}^{K}\alpha_k P_F \Omega_{f_k}}{\mathrm{P}_s\Omega_{h_i}\beta_i} \middle| \begin{matrix} 1-a \\ 0 \end{matrix}\right)dx \\
&+ \frac{\sum_{b=1}^{i-1} B_b}{\Gamma(N-1)\Gamma(b)} \\
&\times \int_0^{\infty} x^{-\frac{1}{2}} G_{0,1}^{1,0}\left(x\left(\frac{1}{\mathrm{P}_s\Omega_{h_i}\beta_i} + \frac{1}{P_R\Omega_g\beta_i} + 1\right) \middle| \begin{matrix} - \\ 0 \end{matrix}\right) \\
&\times G_{1,1}^{1,1}\left(x\frac{\mathrm{P}_s\Omega_{h_j}\sum_{j=i+1}^{N-1}\beta_j}{\mathrm{P}_s\Omega_{h_i}\beta_i} \middle| \begin{matrix} 2-N \\ 0 \end{matrix}\right) \\
&\times G_{1,1}^{1,1}\left(x\frac{\sum_{\ell=1}^{i-1}\beta_\ell P_s\Omega_{h_\ell}}{\mathrm{P}_s\Omega_{h_i}\beta_i} \middle| \begin{matrix} 1-b \\ 0 \end{matrix}\right)dx \\
&+ \frac{\sum_{c=1}^{S} C_c}{\Gamma(N-1)\Gamma(c)} \\
&\times \int_0^{\infty} x^{-\frac{1}{2}} G_{0,1}^{1,0}\left(x\left(\frac{1}{\mathrm{P}_s\Omega_{h_i}\beta_i} + \frac{1}{P_R\Omega_g\beta_i} + 1\right) \middle| \begin{matrix} - \\ 0 \end{matrix}\right) \\
&\times G_{1,1}^{1,1}\left(x\frac{\mathrm{P}_s\Omega_{h_j}\sum_{j=i+1}^{N-1}\beta_j}{\mathrm{P}_s\Omega_{h_i}\beta_i} \middle| \begin{matrix} 2-N \\ 0 \end{matrix}\right) \\
&\times G_{1,1}^{1,1}\left(x\frac{\sum_{s=1}^{S}\theta_s P_M \Omega_{m_s}}{P_R\Omega_g\beta_i} \middle| \begin{matrix} 1-c \\ 0 \end{matrix}\right)dx \qquad (57)
\end{aligned}$$

By means of [63, Eq. (13)], (57) is solved as in (26). Note that α term is set to 1/2 in [63, Eq. (13)]. Likewise, following the similar procedures, the N-th user's EP analytical expressions can be obtained as in (27). Partial fraction decomposition components, which are belong to N-th user in HD mode are presented in below. Where $D_d = y \to -\frac{\lim_{\mathrm{P}_s\Omega_{h_N}\beta_N}}{\sum_{k=1}^{K}\alpha_k P_F \Omega_{f_k}} \times \frac{\partial^{K-d}}{(K-d)!\partial y^{K-d}}\left(1 + y\frac{\sum_{k=1}^{K}\alpha_k P_F \Omega_{f_k}}{\mathrm{P}_s\Omega_{h_N}\beta_N}\right)^{K}\Delta$, $E_e = y \to -\frac{\lim_{P_R\Omega_g\beta_N}}{\sum_{s=1}^{S}\theta_s P_M \Omega_{m_s}} \frac{\partial^{S-e}}{(S-e)!\partial y^{E-e}} \times \left(1 + y\frac{\sum_{s=1}^{S}\theta_s P_M \Omega_{m_s}}{P_R\Omega_g\beta_N}\right)^{S}\Delta$,

$$\Delta = \left[\frac{1}{\left(1 + y\frac{\sum_{k=1}^{K}\alpha_k P_F \Omega_{f_k}}{\mathrm{P}_s\Omega_{h_N}\beta_N}\right)^{K}\left(1 + y\frac{\sum_{s=1}^{S}\theta_s P_M \Omega_{m_s}}{P_R\Omega_g\beta_N}\right)^{S}}\right].$$

Following a similar procedures, the i-th and N-th users' EP analytical expressions for FD mode are obtained as in (28) and (29), respectively. Partial fraction decomposition components, which are belong to i-th user in FD mode are presented as:

$$F_f = y \to -\frac{\lim_{\mathrm{P}_s\Omega_{h_i}\beta_i}}{\sum_{k=1}^{K}\alpha_k P_F \Omega_{f_k}} \times \frac{\partial^{K-f}}{(K-f)!\partial y^{K-f}}\left(1 + y\frac{\sum_{k=1}^{K}\alpha_k P_F \Omega_{f_k}}{\mathrm{P}_s\Omega_{h_i}\beta_i}\right)^{K}\Upsilon,$$

$$G_g = y \to -\frac{\lim_{\mathrm{P}_s\Omega_{h_i}\beta_i}}{\sum_{\ell=1}^{i-1}\beta_\ell \mathrm{P}_s\Omega_{\mathrm{h}_\ell}} \times \frac{\partial^{i-1-g}}{(i-1-g)!\partial y^{i-1-g}}\left(1 + y\frac{\sum_{\ell=1}^{i-1}\beta_\ell \mathrm{P}_s\Omega_{\mathrm{h}_\ell}}{\mathrm{P}_s\Omega_{h_i}\beta_i}\right)^{i-1}\Upsilon$$

$$H = y \to -\frac{\lim_{\mathrm{P}_s\Omega_{h_i}\beta_i}}{P_R\Omega_c}\frac{\partial}{\partial y}\left(1 + y\frac{P_R\Omega_c}{\mathrm{P}_s\Omega_{h_i}\beta_i}\right)\Upsilon$$

$$T_t = y \to -\frac{\lim_{P_R\Omega_g\beta_i}}{\sum_{s=1}^{S}\theta_s P_M \Omega_{m_s}} \times \frac{\partial^{S-t}}{(S-t)!\partial y^{S-t}}\left(1 + y\frac{\sum_{s=1}^{S}\theta_s P_M \Omega_{m_s}}{P_R\Omega_g\beta_i}\right)^{S}\Upsilon$$

$$\Upsilon = \left[\frac{1}{\left(1 + y\frac{\sum_{k=1}^{K}\alpha_k P_F \Omega_{f_k}}{\mathrm{P}_s\Omega_{h_i}\beta_i}\right)^{K}\left(1 + y\frac{P_R\Omega_c}{\mathrm{P}_s\Omega_{h_i}\beta_i}\right)} \times \frac{1}{\left(1 + y\frac{\sum_{\ell=1}^{i-1}\beta_\ell \mathrm{P}_s\Omega_{h_\ell}}{\mathrm{P}_s\Omega_{h_i}\beta_i}\right)^{i-1}\left(1 + y\frac{\sum_{s=1}^{S}\theta_s P_M \Omega_{m_s}}{P_R\Omega_g\beta_i}\right)^{S}}\right].$$

Regarding the N-th user in FD mode,

$$O_o = y \to -\frac{\lim_{\mathrm{P}_s\Omega_{h_N}\beta_N}}{\sum_{k=1}^{K}\alpha_k P_F \Omega_{f_k}} \times \frac{\partial^{K-o}}{(K-o)!\partial y^{K-o}}\left(1 + y\frac{\sum_{k=1}^{K}\alpha_k P_F \Omega_{f_k}}{\mathrm{P}_s\Omega_{h_N}\beta_N}\right)^{K}\Lambda,$$

$$P = y \to -\frac{\lim_{\mathrm{P}_s\Omega_{hN}}\beta_N}{P_R\Omega_c}\frac{\partial}{\partial y}\left(1 + y\frac{P_R\Omega_c}{\mathrm{P}_s\Omega_{h_N}\beta_N}\right)\Lambda$$

$$R_r = y \to -\frac{\lim_{P_R\Omega_g\beta_N}}{\sum_{s=1}^{S}\theta_s P_M \Omega_{m_s}} \times \frac{\partial^{S-r}}{(S-r)!\partial y^{S-r}}\left(1 + y\frac{\sum_{s=1}^{S}\theta_s P_M\Omega_{m_s}}{P_R\Omega_g\beta_N}\right)^S \Lambda$$

$$\Lambda = \left[\frac{1}{\left(1 + y\frac{\sum_{k=1}^{K}\alpha_k P_F \Omega_{f_k}}{\mathrm{P}_s\Omega_{h_N}\beta_N}\right)^K \left(1 + y\frac{P_R\Omega_c}{\mathrm{P}_s\Omega_{h_N}\beta_N}\right)} \times \frac{1}{\left(1 + y\frac{\sum_{s=1}^{S}\theta_s P_M\Omega_{m_s}}{P_R\Omega_g\beta_N}\right)^S}\right].$$

PROOF OF PROPOSITION 3

Revisiting (57), when $\mathrm{P_s} \to 0$, the analytical expressions in the first and second Meijer's G function terms in first, second, and third integral expressions approximate to zero. Therefore, by means of [64, Eq. (07.34.06.0040.01)], the aforementioned Meijer's-G functions approximate to 1. Replacing newly obtained result into the integral expressions in (57) and utilizing [62, Eq. (24)], the final asymptotic EP expression for the i-th user is obtained as in (41). Regarding the N-th user's asymptotic expression in HD mode, following the similar procedures as in the i-th user's asymptotic EP derivations, the N-th user's asymptotic EP expression is obtained as in (42).

Regarding the i-th and N-th users' asymptotic EP expressions in FD mode, following the similar procedures as in the HD mode, the required asymptotic expressions are obtained as in (43) and (44).

REFERENCES

[1] Ericsson, "Ericsson mobility report," 2020. Accessed Feb. 1, 2022. [Online]. Available: https://www.ericsson.com/4adc87/assets/local/mobility-report/documents/2020/november-2020-ericsson-mobility-report.pdf

[2] J. A. Hussein, S. S. Ikki, S. Boussakta, and C. C. Tsimenidis, "Performance analysis of opportunistic scheduling in dual-hop multiuser underlay cognitive network in the presence of cochannel interference," *IEEE Trans. Veh. Technol.*, vol. 65, no. 10, pp. 8163–8176, Oct. 2016.

[3] V. Bankey and P. K. Upadhyay, "Ergodic capacity of multiuser hybrid satellite-terrestrial fixed-gain AF relay networks with CCI and outdated CSI," *IEEE Trans. Veh. Technol.*, vol. 67, no. 5, pp. 4666–4671, May 2018.

[4] Y. Saito, Y. Kishiyama, A. Benjebbour, T. Nakamura, A. Li, and K. Higuchi, "Non-orthogonal multiple access (NOMA) for cellular future radio access," in *Proc. IEEE 77th Veh. Technol. Conf.*, 2013, pp. 1–5.

[5] L. Lei, D. Yuan, C. K. Ho, and S. Sun, "Power and channel allocation for non-orthogonal multiple access in 5G systems: Tractability and computation," *IEEE Trans. Wireless Commun.*, vol. 15, no. 12, pp. 8580–8594, Dec. 2016.

[6] T. M. Cover, "Some advances in broadcast channels," *Adv. Commun. Theory*, vol. 4, pp. 229–260, 1975.

[7] Z. Ding et al., "Application of non-orthogonal multiple access in LTE and 5G networks," *IEEE Commun. Mag.*, vol. 55, no. 2, pp. 185–191, Feb. 2017.

[8] Z. Ding, X. Lei, G. K. Karagiannidis, R. Schober, J. Yuan, and V. K. Bhargava, "A survey on non-orthogonal multiple access for 5G networks: Research challenges and future trends," *IEEE J. Sel. Areas Commun.*, vol. 35, no. 10, pp. 2181–2195, Oct. 2017.

[9] S. M. R. Islam, M. Zeng, O. A. Dobre, and K.-S. Kwak, "Resource allocation for downlink NOMA systems: Key techniques and open issues," *IEEE Wireless Commun.*, vol. 25, no. 2, pp. 40–47, Apr. 2018.

[10] L. Dai, B. Wang, Y. Yuan, S. Han, I. Chih-lin, and Z. Wang, "Non-orthogonal multiple access for 5G: Solutions, challenges, opportunities, and future research trends," *IEEE Commun. Mag.*, vol. 53, no. 9, pp. 74–81, Sep. 2015.

[11] X. Liu and X. Zhang, "NOMA-based resource allocation for cluster-based cognitive industrial Internet of Things," *IEEE Trans. Ind. Informat.*, vol. 16, no. 8, pp. 5379–5388, Aug. 2020.

[12] E. Iradier et al., "Analysis of NOMA-based retransmission schemes for factory automation applications," *IEEE Access*, vol. 9, pp. 29541–29554, 2021.

[13] V. D. Tuong, W. Noh, and S. Cho, "Delay minimization for NOMA-enabled mobile edge computing in industrial Internet of Things," *IEEE Trans. Ind. Informat.*, vol. 18, no. 10, pp. 7321–7331, Oct. 2022.

[14] L. Bing, Y. Gu, T. Aulin, and J. Wang, "Design of autoconfigurable random access NOMA for URLLC industrial IoT networking," *IEEE Trans. Ind. Informat.*, vol. 20, no. 1, pp. 190–200, Jan. 2024.

[15] J. Prados-Garzon, P. Ameigeiras, J. Ordonez-Lucena, P. Muñoz, O. Adamuz-Hinojosa, and D. Camps-Mur, "5G non-public networks: Standardization, architectures and challenges," *IEEE Access*, vol. 9, pp. 153893–153908, 2021.

[16] L. Sarakis et al., "Cost-efficient 5G non-public network roll-out: The affordable5G approach," in *Proc. IEEE Int. Mediterranean Conf. Commun. Netw.*, 2021, pp. 221–227.

[17] M. Wen et al., "Private 5G networks: Concepts, architectures, and research landscape," *IEEE J. Sel. Topics Signal Process.*, vol. 16, no. 1, pp. 7–25, Jan. 2022.

[18] J. N. Laneman, D. N. C. Tse, and G. W. Wornell, "Cooperative diversity in wireless networks: Efficient protocols and outage behavior," *IEEE Trans. Inf. Theory*, vol. 50, no. 12, pp. 3062–3080, Dec. 2004.

[19] Z. Ding, M. Peng, and H. V. Poor, "Cooperative non-orthogonal multiple access in 5G systems," *IEEE Commun. Lett.*, vol. 19, no. 8, pp. 1462–1465, Aug. 2015.

[20] P. Hũu, M. A. Arfaoui, S. Sharafeddine, C. M. Assi, and A. Ghrayeb, "A low-complexity framework for joint user pairing and power control for cooperative NOMA in 5G and beyond cellular networks," *IEEE Trans. Commun.*, vol. 68, no. 11, pp. 6737–6749, Nov. 2020.

[21] Y. Li, M. Jiang, Q. Zhang, Q. Li, and J. Qin, "Cooperative non-orthogonal multiple access in multiple-input-multiple-output channels," *IEEE Trans. Wireless Commun.*, vol. 17, no. 3, pp. 2068–2079, Mar. 2018.

[22] M. F. Kader, M. B. Shahab, and S. Y. Shin, "Exploiting non-orthogonal multiple access in cooperative relay sharing," *IEEE Commun. Lett.*, vol. 21, no. 5, pp. 1159–1162, May 2017.

[23] N. Nomikos, T. Charalambous, D. Vouyioukas, R. Wichman, and G. K. Karagiannidis, "Integrating broadcasting and NOMA in full-duplex buffer-aided opportunistic relay networks," *IEEE Trans. Veh. Technol.*, vol. 69, no. 8, pp. 9157–9162, Aug. 2020.

[24] N. Nomikos, T. Charalambous, D. Vouyioukas, and G. K. Karagiannidis, "When buffer-aided relaying meets full duplex and NOMA," *IEEE Wireless Commun.*, vol. 28, no. 1, pp. 68–73, Feb. 2021.

[25] Y. Zhang, Z. Yang, Y. Feng, and S. Yan, "Performance analysis of a novel uplink cooperative NOMA system with full-duplex relaying," *IET Commun.*, vol. 12, no. 19, pp. 2408–2417, 2018.

[26] W. Jaafar, S. Naser, S. Muhaidat, P. C. Sofotasios, and H. Yanikomeroglu, "Multiple access in aerial networks: From orthogonal and non-orthogonal to rate-splitting," *IEEE Open J. Veh. Technol.*, vol. 1, pp. 372–392, 2020.

[27] V. Özduran, N. H. Mahmood, and H. Chergui, "Power-domain non-orthogonal multiple access based full-duplex one-way wireless relaying network," *Trans. Emerg. Telecommun. Technol.*, vol. 32, no. 10, Oct. 2021, Art. no. e4276.

[28] X. Zou, M. Ganji, and H. Jafarkhani, "Cooperative asynchronous non-orthogonal multiple access with power minimization under QoS constraints," *IEEE Trans. Wireless Commun.*, vol. 19, no. 3, pp. 1503–1518, Mar. 2020.

[29] M. Ranjbar, H. Nguyen-Le, T. Karacolak, and N. H. Tran, "Energy efficiency of NOMA-based wireless networks under Gaussian-mixture interference," in *Proc. IEEE Int. Conf. Commun.*, 2019, pp. 1–6.
[30] V. Özduran, "Co-channel interference effects on downlink power-domain non-orthogonal multiple access," *Wireless Pers. Commun.*, vol. 122, no. 2, pp. 1153–1170, Jan. 2022.
[31] D.-T. Do and M.-S. V. Nguyen, "Outage probability and ergodic capacity analysis of uplink NOMA cellular network with and without interference from D2D pair," *Phys. Commun.*, vol. 37, Dec. 2019, Art. no. 100898.
[32] C. B. Mwakwata et al., "Cooperative scheduler to enhance massive connectivity in 5G and beyond by minimizing interference in OMA and NOMA," *IEEE Syst. J.*, vol. 16, no. 3, pp. 5044–5055, Sep. 2022.
[33] T.-H. Vu, T.-V. Nguyen, T.-T. Nguyen, V. N. Q. Bao, and S. Kim, "Short-packet communications in NOMA-CDRT IoT networks with cochannel interference and imperfect SIC," *IEEE Trans. Veh. Technol.*, vol. 71, no. 5, pp. 5552–5557, May 2022.
[34] A.-T. Le et al., "Power beacon and NOMA-assisted cooperative IoT networks with co-channel interference: Performance analysis and deep learning evaluation," *IEEE Trans. Mobile Comput.*, early access, Nov. 17, 2023, doi: 10.1109/TMC.2023.3333764.
[35] T. Shaik and R. Dhuli, "Outage performance of multi cell-NOMA network over Rician/Rayleigh faded channels in interference limited scenario," *AEU - Int. J. Electron. Commun.*, vol. 145, Feb. 2022, Art. no. 154107.
[36] V. Ozduran, J. M. Cioffi, and S. B. Yarman, "Opportunistic source-pair selection (OSPS) method for multiuser bi-directional wireless relaying networks," in *Proc. IEEE 14th Workshop Signal Process. Adv. Wireless Commun.*, 2013, pp. 565–569.
[37] T.-T. T. Nguyen and D.-T. Do, "Exploiting performance of two-way non-orthogonal multiple access networks: Joint impact of co-channel interference, full-duplex/half-duplex mode and SIC receiver," *Ad Hoc Netw.*, vol. 97, Feb. 2020, Art. no. 102032.
[38] A. Rauniyar, P. E. Engelstad, and O. N. Østerbø, "Performance analysis of RF energy harvesting and information transmission based on NOMA with interfering signal for IoT relay systems," *IEEE Sensors J.*, vol. 19, no. 17, pp. 7668–7682, Sep. 2019.
[39] V. Kumar, B. Cardiff, and M. F. Flanagan, "Fundamental limits of spectrum sharing for NOMA-based cooperative relaying under a peak interference constraint," *IEEE Trans. Commun.*, vol. 67, no. 12, pp. 8233–8246, Dec. 2019.
[40] D.-T. Do, M.-S. V. Nguyen, F. Jameel, R. Jantti, and I. S. Ansari, "Performance evaluation of relay-aided CR-NOMA for beyond 5G communications," *IEEE Access*, vol. 8, pp. 134838–134855, 2020.
[41] T.-H. Vu, T.-V. Nguyen, D. B. d. Costa, and S. Kim, "Performance analysis and deep learning design of underlay cognitive NOMA-based CDRT networks with imperfect SIC and co-channel interference," *IEEE Trans. Commun.*, vol. 69, no. 12, pp. 8159–8174, Dec. 2021.
[42] Y. Liu et al., "Evolution of NOMA toward next generation multiple access (NGMA) for 6G," *IEEE J. Sel. Areas Commun.*, vol. 40, no. 4, pp. 1037–1071, Apr. 2022.
[43] H. Tabassum, M. S. Ali, E. Hossain, M. J. Hossain, and D. I. Kim, "Uplink vs. downlink NOMA in cellular networks: Challenges and research directions," in *Proc. IEEE 85th Veh. Technol. Conf.*, 2017, pp. 1–7.
[44] V. Ozduran, M. Mohammadi, I. S. Ansari, and N. Nomikos, "Performance analysis of uplink non-orthogonal multiple access in the presence of co-channel interference," *IEEE Trans. Veh. Technol.*, vol. 72, no. 9, pp. 11590–11602, Sep. 2023.
[45] T. Rappaport, *Wireless Communications: Principles and Practice*, 2nd ed., (Series Prentice Hall Communications Engineering and Emerging Technologies). Englewood Cliffs, NJ, USA: Prentice Hall, 2002.
[46] Z. Xiang, X. Tong, and Y. Cai, "Secure transmission for NOMA systems with imperfect SIC," *China Commun.*, vol. 17, no. 11, pp. 67–78, Nov. 2020.
[47] G. Im and J. H. Lee, "Outage probability for cooperative NOMA systems with imperfect SIC in cognitive radio networks," *IEEE Commun. Lett.*, vol. 23, no. 4, pp. 692–695, Apr. 2019.
[48] S. S. Ikki and S. Aissa, "Performance analysis of two-way amplify-and-forward relaying in the presence of co-channel interferences," *IEEE Trans. Commun.*, vol. 60, no. 4, pp. 933–939, Apr. 2012.
[49] V. Ozduran and S. B. Yarman, "Impact of the external co-channel interferences over multiuser bi-directional wireless relaying networks-Part I: System description and outage analysis," *Wireless Pers. Commun.*, vol. 78, no. 2, pp. 1277–1295, 2014.
[50] V. Ozduran, E. Soleimani-Nasab, and B. S. Yarman, "Sum-rate based opportunistic relay selection method for a dual-hop multiple half/full-duplex bi-directional wireless relaying networks," in *Proc. IEEE 24th Telecommun. Forum*, 2016, pp. 1–4.
[51] M. K. Simon and M.-S. Alouni, *Digital Communication Over Fading Channels*, 2nd ed., Hoboken, NJ, USA: Wiley, 2005.
[52] T. Nguyen, H. H. K. Duy, H. Nguyen, and M. Voznak, "Throughput analysis in relaying cooperative systems considering time-switching with NOMA," in *Proc. IEEE 41st Int. Conf. Telecommun. Signal Process.*, 2018, pp. 1–4.
[53] H. Q. Ngo, H. A. Suraweera, M. Matthaiou, and E. G. Larsson, "Multipair full-duplex relaying with massive arrays and linear processing," *IEEE J. Sel. Areas Commun.*, vol. 32, no. 9, pp. 1721–1737, Sep. 2014.
[54] I. Gradshteyn and I. Ryzhik, *Tables of Integrals, Series and Products*, 7th ed., Amsterdam, The Netherlands: Elsevier, 2007.
[55] Z. Wang and G. B. Giannakis, "A simple and general parameterization quantifying performance in fading channels," *IEEE Trans. Commun.*, vol. 51, no. 8, pp. 1389–1398, Aug. 2003.
[56] L. J. Rodríguez, N. H. Tran, and T. Le-Ngoc, "Performance of full-duplex AF relaying in the presence of residual self-interference," *IEEE J. Sel. Areas Commun.*, vol. 32, no. 9, pp. 1752–1764, Sep. 2014.
[57] A. Yadav, C. Quan, P. K. Varshney, and H. V. Poor, "On performance comparison of multi-antenna HD-NOMA, SCMA, and PD-NOMA schemes," *IEEE Wireless Commun. Lett.*, vol. 10, no. 4, pp. 715–719, Apr. 2021.
[58] W. Ahsan, W. Yi, Z. Qin, Y. Liu, and A. Nallanathan, "Resource allocation in uplink NOMA-IoT networks: A reinforcement-learning approach," *IEEE Trans. Wireless Commun.*, vol. 20, no. 8, pp. 5083–5098, Aug. 2021.
[59] N. Nomikos, M. S. Talebi, T. Charalambous, and R. Wichman, "Bandit-based power control in full-duplex cooperative relay networks with strict-sense stationary and non-stationary wireless communication channels," *IEEE Open J. Commun. Soc.*, vol. 3, pp. 366–378, 2022.
[60] A. Papoulis and U. Pillai, *Probability, Random Variables and Stochastic Processes*, 4th ed., New York, NY, USA: McGraw-Hill, 2001.
[61] I. S. Gradshteyn and I. M. Ryzhik, *Tables of Integrals, Series and Products*, 7th ed., Amsterdam, The Netherlands: Elsevier Inc., 2007.
[62] V. S. Adamchik and O. I. Marichev, "The algorithm for calculating integrals of hypergeometric type functions and its realization in REDUCE systems," in *Proc. Int. Symp. Symbolic Algebr. Comput.*, 1990, pp. 212–224.
[63] N. H. Mahmood, I. S. Ansari, P. Popovski, P. Mogensen, and K. A. Qaraqe, "Physical-layer security with full-duplex transceivers and multiuser receiver at eve," *IEEE Trans. Commun.*, vol. 65, no. 10, pp. 4392–4405, Oct. 2017.
[64] "Wolfram Research," Aug. 2023. [Online]. Available: https://functions.wolfram.com

VOLKAN ÖZDURAN (Member, IEEE) received the graduation degree from the department of Electronics, Soke Technical High School, Aydin, Turkey, in 1997, the A.Sc. degree in industrial electronics (with First Hons.) and the B.Sc., M.Sc., and Ph.D. degrees in electrical and electronics engineering from Istanbul University, Istanbul, Turkey, in 2002, 2005, 2008, and 2015, respectively. During his Ph.D. studies he was with the Department of Electrical Engineering, Stanford University, Stanford, CA, USA, Department of Electrical Engineering, Dynamic Spectrum Management (DSM) Research group, California Institue of Technology, Pasadena, CA, and Department of Electrical Engineering, Princeton University, Princeton, NJ, USA. His research focuses on various aspects of the 6G wireless networks. He received the Docent title from the Turkish Interuniversity Council, Ankara, Turkey in 2022.

NIKOLAOS NOMIKOS (Senior Member, IEEE) received the diploma in electrical engineering and computer technology from the University of Patras, Patras, Greece, in 2009, and the M.Sc. and Ph.D. degrees from the Information and Communication Systems Engineering Department, University of the Aegean, Samos, Greece, in 2011 and 2014, respectively. He is currently a Senior Researcher with the Department of Ports Management and Shipping, National and Kapodistrian University of Athens, Zografou, Greece. His research interests include cooperative communications, non-orthogonal multiple access, full-duplex communications, and machine learning for wireless networks optimization. Dr. Nomikos is an Editor of IEEE TRANSACTIONS ON COMMUNICATIONS and Associate Editor for *Frontiers in Communications and Networks*. He is a Member of the IEEE Communications Society and the Technical Chamber of Greece.

EHSAN SOLEIMANI-NASAB (Member, IEEE) received the B.Sc. degree in electrical engineering from the Iran University of Science and Technology, Tehran, Iran, in 2006, and the M.Sc. and Ph.D. degrees in communication systems from the K. N. Toosi University of Technology, Tehran, in 2009 and 2013, respectively. From April 2012 to October 2012, he was a Visiting Researcher with the Department of Signals and Systems, Chalmers University of Technology, Gothenburg, Sweden. From June 2014 to August 2014, he was a Research Associate with the Department of Electrical and Electronics Engineering, Özyegin University, Istanbul, Turkey. Since 2014, he has been with the Graduate University of Advanced Technology, Kerman, Iran, where he is currently an Associate Professor. From 2022 to 2023, he was a Guest Researcher with the Department of Electrical and Electronics Engineering, Koc University, Istanbul. He has authored or coauthored more than 60 journal and conference publications. His research interests include optical wireless communications, radio wireless communications, and signal processing in communications. He was with the technical program committees for various IEEE conferences. He is an active reviewer for various IEEE Transactions and other journals.

IMRAN SHAFIQUE ANSARI (Senior Member, IEEE) received the B.Sc. (with First Hons.) degree in computer engineering from the King Fahd University of Petroleum and Minerals, in 2009, and the M.Sc. and Ph.D. degrees from the King Abdullah University of Science and Technology, in 2010 and 2015, respectively. Since 2018, he has been a Lecturer (Assistant Professor) with the University of Glasgow, Glasgow, U.K. He has authored or coauthored more than 100 journal and conference publications. His research interests include free-space optics (FSO), satellite communications, underwater communications, physical layer secrecy issues, and reconfigurable intelligent surfaces / intelligent reflective surfaces (RIS / IRS). He has been affiliated with IEEE since 2007 and has served in various capacities. He is with IEEE European Public Policy Committee (2023–2024) and IEEE LEO SatS Future Directions since 2022. He was with the IEEE Nominations and Appointments (N&A) Committee (2020–2021) and IEEE Communication Society Young Professionals (ComSoc YP) Board (2016–2021). He is part of the IEEE 5G Tech Focus Publications Editorial Board since 2017. He is an active reviewer of EPSRC research grants, various IEEE Transactions and various other journals. He was a TPC for various IEEE conferences. He has co-organized the GRASNET'2016, 2017, 2018 workshops in conjunction with IEEE WCNC'2016, 2017 and IEEE Globecom 2018. He was the recipient of appreciation for an exemplary reviewer of IEEE TRANSACTION ON COMMUNICATIONS (TCOM) in 2016 and 2018, exemplary reviewer of IEEE WIRELESS COMMUNICATIONS LETTERS (WCL) in 2014 and 2017, Postdoctoral Research Award (PDRA) (first cycle) with Qatar National Research Foundation (QNRF) in 2014, KAUST Academic Excellence Award (AEA) in 2014, and IEEE Richard E. Merwin student scholarship award in 2013.

PANAGIOTIS TRAKADAS received the Dipl.-Ing. degree in electrical and computer engineering and the Ph.D. degree from the National Technical University of Athens, Athens, Greece. In the past, he was with the Hellenic Aerospace Industry (HAI), as a Senior Engineer, on the design of military wireless telecommunications systems, and the Hellenic Authority for Communications Security and Privacy, where he was holding the position of the Director of the Division for the Assurance of Infrastructures and Telecommunications Services Privacy. He is currently an Associate Professor with the National and Kapodistrian University of Athens, Zografou, Greece. He has been actively involved in many EU FP7 and H2020 Research Projects. He has authored or coauthored more than 130 papers in magazines, journals, and conference proceedings. His research interests include the fields of wireless and mobile communications, wireless sensor networking, network function virtualization, and cloud computing. He is a Reviewer of several journals, including IEEE TRANSACTIONS ON COMMUNICATIONS and IEEE TRANSACTIONS ON ELECTROMAGNETIC COMPATIBILITY.